C.P. No. 304
(17,990)
A.R C. Technical Report

C.P. No. 304
(17,990)
A.R.C. Technical Report

MINISTRY OF SUPPLY

AERONAUTICAL RESEARCH COUNCIL

CURRENT PAPERS

Three-Dimensional Wind-Tunnel Tests of a 30° Jet Flap Model

By

J. Williams, M.Sc., Ph.D., and

A. J. Alexander, B.Sc.,

of the Aerodynamics Division, N.P.L.

LONDON · HER MAJESTY'S STATIONERY OFFICE

1957

EIGHT SHILLINGS NET

Three-Dimensional Wind-Tunnel Tests of a 30° Jet Flap Model

- By -
J. Williams, M.Sc., Ph.D.
and
A. J. Alexander, B.Sc.
of the Aerodynamics Division, N.P.L.

9th November, 1955

SUMMARY

As a first investigation of finite aspect ratio effects in relation to the jet flap scheme, pressure plotting experiments were made on a small-scale model, with a 12½% thick wing section already tested under two-dimensional conditions at the N.G.T.E. The spanwise distribution of 'pressure lift' loading induced by T.E. blowing was evaluated by chordwise integration of the surface static pressures, and followed closely that which would be expected for a conventional wing at incidence (without T.E. blowing). The total lift, drag and pitching moments were derived for values of jet momentum coefficient C_J up to 2 at wing incidences between -5° and 20°, and up to 5 at zero incidence, by summing the corresponding integrated pressure forces and jet reaction components.

CONTENTS

1./

Published with permission of the Director, National Physical Laboratory

1. Introduction

The jet flap scheme developed at the N.G.T.E.[1] is essentially a means of producing an asymmetry of flow about a wing in order to increase lift at constant wing incidence, without recourse to mechanical devices such as large T.E. flaps. Air is ejected with high velocity at an angle θ to the chord-line, through a narrow spanwise slot at the wing T.E. In the so-called 'shrouded jet flap', a small hinged T.E. flap is included merely to turn the jet through the required angle by Coanda effect, instead of inclining the direction of the blowing slot to the chord line. The jet-flap scheme may be contrasted with blowing over normal size T.E. flaps, where the asymmetry of the flow is basically engendered by the flap deflection, and the blowing prevents flow separation over the flap nose, thus ensuring that the flap attains its theoretical efficiency* (see Fig.1 of Ref.3). Even in this case, if the blowing momentum is increased beyond that required to prevent flow separation, the lift is also further increased (supercirculation) by the effective extension of the flap chord (or downward displacement of the dividing streamline extending from the T.E. of the flap[4]).

Extensive two-dimensional wind-tunnel tests on 12½% thick elliptic sections have been made at the N.G.T.E.[2] for various jet deflection angles θ up to and including 90°. At the request of the A.R.C. Performance Sub-Committee, tests on a three-dimensional jet flap model were carried out at the N.P.L. to obtain quickly some idea of the magnitude of finite aspect ratio effects†. A small pressure-plotting model of rectangular planform, with a 12½% thick elliptic section and a jet angle of 31.3°, was provided by N.G.T.E. and was mounted with a plate at one end to give an effective aspect ratio slightly less than 3.0 (see § 2). The lift, drag and pitching moment forces were calculated from measurements of the surface static pressures and the jet reaction. For completeness, tests were also made on the same wing with a second end-plate added, in an attempt to approach two-dimensional flow conditions (see § 2).

2. Experimental Set-up

The model was made of metal, with a chord c of 8 inches and with a span s of 12 inches excluding the ellipsoidal tip fairing which added a further 0.25 inches. A turntable, attached at the model root, rotated about the mid-chord axis in a fixed end-plate as illustrated in Fig.1a; the end-plate extended about 0.8 chord upstream of the wing L.E., two chords downstream of the T.E. (jet exit), one chord vertically above the zero-incidence chord-line and two chords below. Fig.2a, which was derived from the theoretical results of Ref.4, gives the effective aspect ratio of the wing as 2.75 for the appropriate ratio of wing span to end-plate height. The set-up of the supplementary experiments, with the ellipsoidal tip removed and a second end-plate added, did not represent strictly two-dimensional conditions. With the present end-plate size, which was limited by

structural/

---

*The quantity requirements to achieve a moderate lift by blowing over a normal size T.E. flap are considerably less than those needed with the simple jet flap at the same angle.

†Provisional conclusions were communicated to the A.R.C. Performance Sub-Committee in February, 1954, immediately the tests were completed, and advance copies of some of the graphs contained herein have already been given very limited circulation.

structural and accessibility considerations, the loading was sensibly constant across the span but according to Fig.2a, the effective aspect ratio was only 6.8.

For the measurement of surface static pressures, 26 tappings were provided at each of the four spanwise stations 0.2s, 0.5s, 0.8s and 0.95s from the wing root, closely spaced near the L.E. and T.E. of the model. Some static pressure tappings were also included in the end-plate at the wing root but these were only useful for general guidance. Unfortunately, it was not possible to incorporate static tubes in the blowing slot walls. The upper lip of the blowing slot was located at the T.E. of the elliptic section with the lower lip just on the undersurface to give a mean slot width w of 0.025 in., i.e., w/c = 0.003; the spanwise variation was less than 0.0025 in. N.G.T.E. measurements showed that at zero wind-speed the jet issued at an angle 31.3° to the chord-line, with no observable variation spanwise or change with jet efflux over the practical range. The internal structure of the model is shown in Fig.1b.

The model was located centrally in the N.P.L. Low Turbulence Wind-Tunnel (regular 16-sided cross-section, 7 ft height), so that the tunnel interference effects were small. The general arrangement of the model and the external ducting to the Broom-Wade compressor unit is depicted in Fig.1a. A simple pitot comb traverse gear was employed to explore briefly the development of the jet wake (see Fig.1c). The jet could be straddled at any spanwise location and at distances downstream up to three chords behind the T.E; the axis of the comb could be aligned along the local mean direction of the jet flow. Detailed explorations were not possible, however, owing to shortage of tunnel time and lack of a sufficiently closely spaced pitot comb.

The calibration curve given in Fig.2b, of jet reaction J against the jet total pressure measured in the blowing duct, was used to derive the values of the non-dimensional jet reaction coefficient C_J ($\equiv J/\frac{1}{2}\rho_o U_o^2 S$). The curve was determined at the N.G.T.E. from balance measurements of thrust with the model at zero incidence and with zero wind-tunnel speed, a correction being applied to allow for the static pressure distribution arising from the flow induced about the model by the jet efflux.

3. Range of Tests and Reduction of Observations

Most of the wind tunnel tests were carried out at a windspeed of 100 ft/sec ($R = 0.1 \times 10^6$), when the available air supply permitted C_J - values up to 0.5 to be used. Higher values of C_J were obtained by reducing the windspeed to 50 ft/sec ($C_J < 2.1$) and to 30 ft/sec ($C_J < 4.8$). Observations were first made with the three-dimensional model at zero incidence and C_J - values up to 4.8. Transition wires were located on the front upper and lower surfaces of the model, at 0.2c behind the L.E., as far forward as possible without causing interference at the closely spaced static holes in the wing nose. Similar experiments were then made at incidences ranging between -5° and 20° for C_J values up to 2.1, both with and without transition wires. Unless otherwise stated the results discussed in the text and plotted in the graphs refer to those obtained with transition wires.

The lift coefficient C_L on the wing may be regarded as comprising the vertical component $C_J \sin(\theta + \alpha)$ of the jet reaction at the nozzle and the vertical 'pressure force' C_{Lp} arising from the airflow over the aerofoil surface. Thus we write

$$\left.\begin{aligned} C_L &= C_J \sin(\theta + \alpha) + C_{Lp} \\ C_D &= -C_J \cos(\theta + \alpha) + C_{Dp} \\ C_M &= -\tfrac{2}{c} C_J + C_{Mp} \end{aligned}\right\} \quad \ldots\ldots(1)$$

where/

where n is the perpendicular distance from the point about which moments are taken onto the extended centre-line of the jet nozzle. For moments about mid-chord, as quoted for the present tests, $n/c \simeq \frac{1}{2} \sin\theta$. The sectional pressure-force coefficients were obtained from the measured static pressures by chordwise integration. The overall force coefficients were then derived by integration across the span, and for convenience were based on the area S of the rectangular plan-form excluding the small ellipsoidal tip[x]. Some simplifying assumptions had to be made for the chordwise integration of the static pressures close to the T.E. since there were no static pressure holes inside the slot throat. Although the resulting error in the lift coefficients is insignificant, this may not be so for the pitching moment and drag coefficients under all conditions.

The quasi two-dimensional experiments, made with the ellipsoidal tip removed and a second end-plate added, covered roughly the same ranges of C_J and incidence as those tested on the three-dimensional model. It was first checked that the set-up gave sensibly constant loading across the span, i.e., nominally two-dimensional flow, for a few representative conditions. Then for the remainder of the tests, the static pressures were recorded only at the mid-span section and the pressure force coefficients evaluated therefrom.

4. Three-Dimensional Model Results

4.1 Lift

The spanwise distribution of 'pressure lift' loading induced by T.E. blowing, with the wing at zero incidence, seems little different from that given by simple lifting-line theory (see Fig.3a) or that due to wing incidence without blow (Fig.3b).

The total lift C_L at zero wing incidence is plotted against $C_J^{\frac{1}{2}}$ in Fig.4a, both with and without transition wires and for various windspeeds. At C_J-values below unity, the experimental results lie reasonably close to the straight line $C_L = 1.4\, C_J^{\frac{1}{2}}$, and at higher C_J-values are slightly above this. The relative magnitudes of the jet reaction and pressure force contributions to the total lift are also indicated. Curves of C_L against $C_J^{\frac{1}{2}}$ for other incidences are plotted in Fig. 4b for the case with transition wires; the slope $dC_L/dC_J^{\frac{1}{2}}$ at a prescribed C_J is seen to increase with incidence. The C_L-values obtained without transition wires are in most instances not more than 0.1 different from those with.

Lift-incidence curves for a range of C_J-values with transition wires are shown in Fig.5. As C_J is increased from zero there is no significant loss in stalling incidence; at C_J-values above unity there is even some increase in stalling incidence which, though possibly peculiar to the low Reynolds number and particular wing configuration of the tests, is at least encouraging. The value of $dC_L/d\alpha$ for small incidences rises steadily as C_J increases, from 0.055/deg without blow to about 0.1/deg at $C_J = 2$. The increase is roughly proportional to $C_J^{\frac{1}{2}}$, and is made up of contributions from both the jet reaction and pressure force components. With α measured in degrees,

$$dC_L/d\alpha = 0.0175\, C_J \cos(\theta + \alpha) + dC_{Lp}/d\alpha \qquad \ldots\ldots(2)$$

$$\simeq 0.015\, C_J + dC_{Lp}/d\alpha \text{ for small } \alpha \qquad \ldots\ldots(3)$$

The removal of the transition wires had little effect on $dC_L/d\alpha$, except for the results without blowing, when the value became extraordinarily high. This seemed to be associated with the presence of a thin laminar boundary layer right back to the T.E. at the low test Reynolds number combined with the unusual slotted T.E. shape.

4.2/

---

[x] The tip increased the wing area by only about $1\frac{1}{2}\%$.

4.2 Pitching Moment

Fig.6 gives curves of total pitching moment C_M about the half-chord axis plotted against the corresponding total lift C_L, for a range of values of α and C_J, from the tests with transition wires.

Probably not more than broad conclusions should be drawn from the results, in view of the few static pressure holes in the vicinity of the slot. It is seen that the mean slope $(dC_M/dC_L)_{C_J}$ of the curves for constant C_J (α varied) is about 0.25 at low but non-zero values of C_J, so that the aerodynamic centre is located close to the quarter-chord position. As C_J increases, the value of $(dC_M/dC_L)_{C_J}$ decreases so that the aerodynamic centre tends to move further aft, say by about 0.04c as C_J is raised from 0.2 to unity. The C_M - C_J curves for zero C_J are, however, somewhat unusual in that the slopes both with and without transition wires differed appreciably from 0.25, being respectively greater and less. This peculiar behaviour in the absence of blowing was again accredited to the unconventional T.E. shape and low Reynolds number of the tests.

As C_J increases with α constant, the nose-down pitching moment becomes steadily larger*, because the induced suction forces on the wing upper surface are much higher near the T.E. than the L.E. (see later discussion on pressure distributions). The chordwise location of the centre of total lift is plotted against C_L in Fig.7, and in general moves rearward appreciably as C_J is increased at constant incidence or as the incidence is decreased at constant C_J.

4.3 Drag

The total drag coefficient C_D on the wing, as defined by equation(1) of §3, is plotted against C_J in Fig.8a, for a range of wing incidences both with and without transition wires. Again the drag results do not warrant more than a qualitative examination.

It will be recalled that the drag is made up of the chordwise components of the direct jet reaction and the pressure forces on the aerofoil surface; the relative magnitudes of the two contributions are indicated in Fig.8a for the zero incidence case. Thus, without blowing, C_D includes the conventional form drag of the wing sections and the induced drag arising from downwash effects, but excludes the skin-friction drag. With blowing, we might therefore regard C_D as comprising a chordwise component $-C_J \cos(\theta + \alpha)$ from the direct jet reaction, a form drag together with any recovery of thrust which manifests itself in the pressure distribution, and an induced drag resulting from downwash effects over the wing. For ideal conditions, i.e., potential flow in the mainstream flow and no mixing, it can be shown that the direct jet reaction and thrust recovery terms taken together contribute the amount $-C_J$ corresponding to the gross thrust. In our measurements the so-called form drag, induced drag and thrust recovery terms are of necessity lumped together as pressure drag. Fig.8a shows that the rate of decrease in C_D with C_J is appreciably less than the amount $C_J \cos(\theta + \alpha)$ associated with the direct jet reaction. Thus, because of the low aspect ratios and small jet angle, the combined form and induced drag contributions to the pressure drag completely outweigh and mask any negative contribution arising from thrust recovery.

For comparisons with the pressure drag associated with more conventional methods of producing pressure lift on a wing, namely by incidence and camber, the value of C_{Dp} for the present jet flap wing

has/

---

*On a complete aircraft with tail this could at least be partially trimmed out by the increased downwash over the tail.

has been plotted against C_{Lp}^2. Fig.8b, for the wing at zero incidence shows that for C_J-values below 0.5 the points lie close to the straight line

$$C_{Dp} = 0.013 + 0.14\ C_{Lp}^2$$

while for C_J-values up to 2 the value of C_{Dp} does not exceed $0.013 + 0.16\ C_{Lp}^2$. Fig.8c, giving results for other incidences, shows that up to 11° the trend is also much the same. The combined form and induced drags of a conventional wing of aspect ratio 2.75 producing corresponding pressure lifts at the same Reynolds number would not in fact be greatly different from the above (see § 6).

4.4 General Flow Characteristics and Pressure Distributions

Tuft and china clay observations were made to visualise the flow about the model. For C_J-values up to 2.1, with the wing at zero incidence, no separation was evident on the upper surface due to the adverse pressure gradients at the front[7]. As the wing incidence was increased a small bubble of separated flow appeared, at the inboard sections first, being formed by separation of the laminar boundary layer close to the L.E. with subsequent reattachment as a turbulent boundary layer ahead of the transition wire. Without blowing, the bubble did not expand appreciably chordwise until the incidence exceeded 10°, after which the position of reattachment moved steadily rearwards, again at the inboard sections first. The behaviour with blowing operative was similar, but the wing incidence at which the bubble began to expand decreased somewhat as C_J was increased.

Some representative pressure distributions with the wing at zero incidence and transition wires on are shown in Figs.9a and 9b for the chordwise sections at $y/s = 0.20$ and $y/s = 0.95$, and selected C_J-values up to 2.1. It is seen that they are similar in shape to the pressure distributions on the main part of a wing when a T.E. flap is deflected. In order to obtain some idea of the variation in pressure distribution with incidence as well as C_J, the values of the peak suctions occurring near the L.E. and T.E. of the two chordwise sections have been plotted against incidence for C_J-values ranging up to 2.1 (see Fig.10). As the incidence increases at constant C_J the peak suction on the nose grows more rapidly at the inboard than the outboard section, so flow separation may be expected earlier inboard which agrees with the deduction from flow visualisation experiments. Furthermore, although the peak suction near the T.E. of the outboard section grows with increasing incidence, that at the T.E. of the inboard section varies little at first and eventually diminishes. As C_J increases at constant incidence, the T.E. peak suctions grow much more rapidly than those near the L.E., partly because the latter are much reduced by downwash effects.

Some total head traverses of the jet were carried out at various distances downstream of the T.E. and at a few spanwise locations, but unfortunately the tests had to be severely limited. Fig.11a shows the mean line of the jet (locus of maximum total head) and also the distribution of the total head in the wake downstream of the mid-span station (6 in. from the root), for the wing at zero incidence with $C_J = 0.5$. It is seen that the width of the wake increases rapidly near the slot exit, being about 1 in. at a quarter-chord behind the T.E., by which time the inclination of the mean-line to the chord has fallen to about 15°. Fig.11b compares a few measurements of the mean-line of the jet downstream of the mid-span station with those further outboard. Spanwise variations are clearly evident further outboard than 10 in. from the root, i.e., beyond about 85% span.

5./

[7] In the absence of transition wires, laminar flow seemed to persist right back to the T.E.

5. Quasi Two-Dimensional Model Results

The pressure force coefficients were derived from static pressure measurements at the mid-span section only, since the lift loading was sensibly constant across the span‡. The curves of total lift, pitching moment and drag for the quasi two-dimensional model (effective aspect ratio ≈ 6.8) are generally similar in character to those already discussed for the three-dimensional model.

At C_J-values below unity, the results for the total lift C_L at zero incidence both with and without transition wires, lie reasonably close to the straight line $C_L = 1.7\ C_J^{\frac{1}{2}}$ and at higher C_J-values are slightly above this (see Fig.12a). Curves of C_L against $C_J^{\frac{1}{2}}$ for other incidences derived from tests with transition wires are plotted in Fig.12b. Lift-incidence curves for a range of C_J-values are also shown in Fig.13, the value of $dC_L/d\alpha$ at small incidences rising steadily from about 0.075/deg without blow to 0.15/deg at $C_J = 2$.

The total pitching moment C_M about the half-chord axis is plotted against C_L for a range of C_J in Fig.14. At low C_J the aerodynamic centre is located close to the quarter-chord position and moves rearward about 0.06c as C_J increases from 0.2 to unity. The chordwise location of the centre of total lift also moves rearward in general as C_J increases with α constant, or as α decreases at constant C_J (see Fig.15).

The total drag coefficient C_D is plotted against C_J in Fig.16a for a range of incidences. It is immediately evident that the rate of decrease of C_D with C_J at zero incidence is less than $C_J \cos\theta$, so that the increase in pressure drag due to the so-called form and induced drag components again outweighs any decrease from the thrust recovery term. The values of the pressure drag, with the wing at zero incidence and with front transition wires, satisfy fairly well the relation

$$C_{Dp} = 0.015 + 0.068\ C_{Lp}^2$$

for C_J values up to 2 (see Fig.16b). This relation also holds with the wing at higher incidences, up to at least 6.5° (see Fig.16c), and is not far different from that for the combined induced and form drags of a conventional wing of aspect ratio 6.8 giving the same pressure lift (see § 6).

Some representative pressure distributions for the mid-span section with the wing at zero incidence and transition wires on are given in Fig.17 for a range of C_J-values. As the incidence increases at constant C_J, the peak suction near the T.E. varies little at first but eventually diminishes (see Fig.18); the value at moderate incidences is little different from that measured for the inboard sections of the three-dimensional model (c.f. Fig.10). The peak suction at the nose of course increases with incidence, until a certain maximum value ($-C_p \simeq 5$) is reached. For any prescribed incidence below that corresponding to this maximum value, the peak suction in general exceeds that measured on the three-dimensional model. The maximum is reached at a lower incidence, as would be expected because of the smaller downwash effects, but its value is not vastly different.

The mean line of the jet and the distribution of total head in the wake downstream of the T.E. are plotted in Fig.19 for the wing at zero incidence with C_J-values of 0.18 and 0.5.

6./

---

‡This was also checked for us theoretically by Miss Weber of the R.A.E., Farnborough.

6. General Conclusions on Finite Aspect Ratio Effects

The investigation described in the present report was a preliminary and first attempt to explore the effects of finite aspect ratio on the jet flap scheme. The experiments were not intended to provide comprehensive data for detailed project studies nor to establish fundamental postulates for a three-dimensional jet flap theory, but simply to give some idea of the magnitude of finite aspect ratio effects, particularly in relation to lift. Nevertheless, in summarising the results obtained for wing aspect ratios in the vicinity of 2.75 and 6.8, it is at least worth considering them in the light of simple aspect ratio correction factors for conventional wings without T.E. blowing*.

6.1 Summary of Experimental Results

(a) Total Lift (Figs.4 and 12) - For zero incidence, and $C_J < 1$, the results for the aspect ratio 2.75 and 6.8 wings lie close to the values

$$C_L = 1.4\ C_J^{\frac{1}{2}} \text{ and } C_L = 1.7\ C_J^{\frac{1}{2}} \text{ respectively,}$$

and are about 0.6 and 0.7 respectively of the corresponding N.G.T.E. two-dimensional values[2]. The appropriate values of the aspect ratio correction factor $[1 + (a_o/\pi Ae)]^{-1}$ for lift on conventional wings are 0.58 and 0.77 respectively, assuming elliptic loading ($e = 1$) and a sectional lift curve slope a_o equal to the flat-plate value of 2π.

(b) Pressure Drag (Figs.8 and 16) - For zero incidence and $C_J < 1$, the results for the aspect ratio 2.75 and 6.8 wings satisfy approximately the relations

$$C_{Dp} = 0.013 + 0.14\ C_{Lp}^2 \text{ and } C_{Dp} = 0.015 + 0.068\ C_{Lp}^2$$

respectively. The corresponding induced (pressure) drag $C_{Lp}^2/\pi Ae$ for conventional wings producing the lift C_{Lp} takes the values $0.116\ C_{Lp}^2$ and $0.047\ C_{Lp}^2$ respectively, assuming elliptical loading ($e = 1$). The remaining contribution ($\doteq 0.015 + 0.02\ C_{Lp}^2$) could reasonably be accounted for as sectional form drag in both cases. The approximate agreement between the measured pressure drags and the corresponding conventional drag estimates (induced and form) may well be fortuitous, but at least it seems that the pressure drag on the jet flap wing is not likely to be much larger than that of a conventional wing producing the same pressure lift.

(c) Lift-Incidence Curves (Figs.5 and 13) - For both aspect ratios the measured slopes $dC_L/d\alpha$ at constant C_J and small incidences are about doubled as C_J is raised from near zero to 2.0, and the increase is roughly proportional to $C_J^{\frac{1}{2}}$. There is also no significant loss in stalling incidence ($dC_L/d\alpha = 0$) as C_J is raised.

(d) Pitching Moments (Figs.6, 7, 14 and 15) - For small C_J-values, the aerodynamic centre is located near the quarter-chord position, and the centre of total lift at zero incidence lies close to half-chord. Both move steadily rearward as C_J increases at constant incidence.

6.2 Fundamental Considerations

The foregoing correlation of the pressure drag C_{Dp} in terms of C_{Lp}^2 would at first sight imply that

(a)/

---

*i.e., with the lift produced by incidence or camber.

(a) the downwash due to trailing vorticity affects only the pressure force contribution to the lift vector.

(b) the downwash is generated only by the pressure lift.

The general consensus of opinion held at present supports the first postulate that the pressure lift only is affected, since there seems little reason for the downwash to have other than small effects on the jet reaction. However, in preference to the second, it is generally considered[1] that the downwash results from the reaction of the total lift on the mainstream. On this basis, the effective downwash angle at the wing is by conventional arguments $\phi = C_L/\pi Ae$ and the corresponding induced drag contribution to the pressure drag is $C_{Lp}\, C_L/\pi Ae$, where e represents an efficiency factor which would be unity for a wing at incidence without blowing and with elliptic loading. The measured C_{Dp} values are plotted against $C_{Lp}\, C_L$ in Figs.8d and 16d respectively for the aspect ratio 2.75 and 6.8 wings at zero incidence. It is seen that, as C_J increases, the efficiency factor e satisfying a relation of the type

$$C_{Dp} = \text{const.} + (C_L\, C_{Lp}/\pi Ae)$$

also increases[/]. This would imply an effective increase in aspect ratio with increasing C_J possibly due to the interaction between the jet and the mainstream[1]. Thus, in general, e may well be dependent on C_J, θ and A as well as on planform.[+]

As far as aspect ratio corrections for lift are concerned it can likewise be argued that the jet produces effectively a change in the sectional no-lift angle, that the pressure lift only is affected by downwash, but that the latter should again be based on the total lift. Simple formulae are then readily obtainable for the pressure lift and the slope of the pressure lift-incidence curve in terms of the corresponding two-dimensional values for the same C_J, but these again involve the product Ae, i.e., the effective aspect ratio.

6.3 Further Work Proposed

Although some attempts have been made to analyse the present experimental data in terms of the above and other arguments, the experiments were not sufficiently comprehensive to permit a careful resolution of fundamental considerations on aspect ratio effects. For this reason, further experiments are proposed on a larger scale model with variable aspect ratio and jet angle. It is intended to determine the forces by balance as well as pressure-plotting measurements, and to make a detailed study of the nature of the three-dimensional flow.

References/

/Note that the value of e derived in this case is lowered by the form drag contribution.

+It can also be argued that the total lift should be used throughout to derive the induced drag, giving a formula of the type $C_{Dp} = \text{const} + (C_L^2/\pi Ae)$. Detailed theoretical studies are being carried out at the R.A.E., Farnborough, to clarify these points.

References

No.	Author(s)	Title, etc.
1	I. M. Davidson	The jet flap. R.Ae.Soc. Lecture, October, 1955.
2	N. A. Dimmock	An experimental introduction to the jet flap. N.G.T.E. Rep.R.175. July, 1955. A.R.C. 18,186.
3	J. Williams	An analysis of aerodynamic data on blowing over T.E. flaps for increasing lift. A.R.C. C.P.209, September, 1954.
4	W. Mangler and J. Rotta	Theory of the three-dimensional aerofoil. Part I - Theory of the supporting line. AVA Monograph F_1. M.O.S. R. & T.1023. A.R.C. 11,553 November, 1947.

Acknowledgements

The writers are much indebted to N.G.T.E. for constructing the model and providing the pumping equipment, in particular to Mr. N. A. Dimmock. The lengthy computations and graphical integrations associated with the reduction of the observations were carried out by Miss E. M. Love, Miss L. N. Esson and Miss A. K. Kernaghan, and the wake traverse gear was designed by Mr. N. Marcus, all of the Aerodynamics Division, N.P.L.

List of Symbols

a_o — slope of two-dimensional total lift-incidence curve

A — wing aspect ratio

c — wing chord

C_{Lp}, C_{Dp}, C_{Mp} — Pressure lift, drag and pitching moment coefficients (about $\frac{1}{2}$-chord); derived by integration of pressure forces on aerofoil

C_L, C_D, C_M — Total lift, drag and pitching moment coefficients (about $\frac{1}{2}$-chord); derived by adding direct jet reaction components to pressure forces on aerofoil. See eqn.(1), § 3)

C_J/

C_J jet coefficient = $J/\frac{1}{2}\rho_o U_o^2 S$

C_p static pressure coefficient = $(p - p_o)/\frac{1}{2}\rho_o U_o^2$

e wing efficiency factor. See §6.

h end-plate height

J total jet reaction

p static pressure

p_o, ρ_o, U_o mainstream static pressure, density, and velocity

R mainstream Reynolds number based on wing chord

s span of wing (excluding small ellipsoidal tip)

S area of wing (excluding small ellipsoidal tip)

w width of blowing slot

x chordwise distance

y spanwise distance from root

α wing incidence

θ jet deflection angle relative to wing chord-line

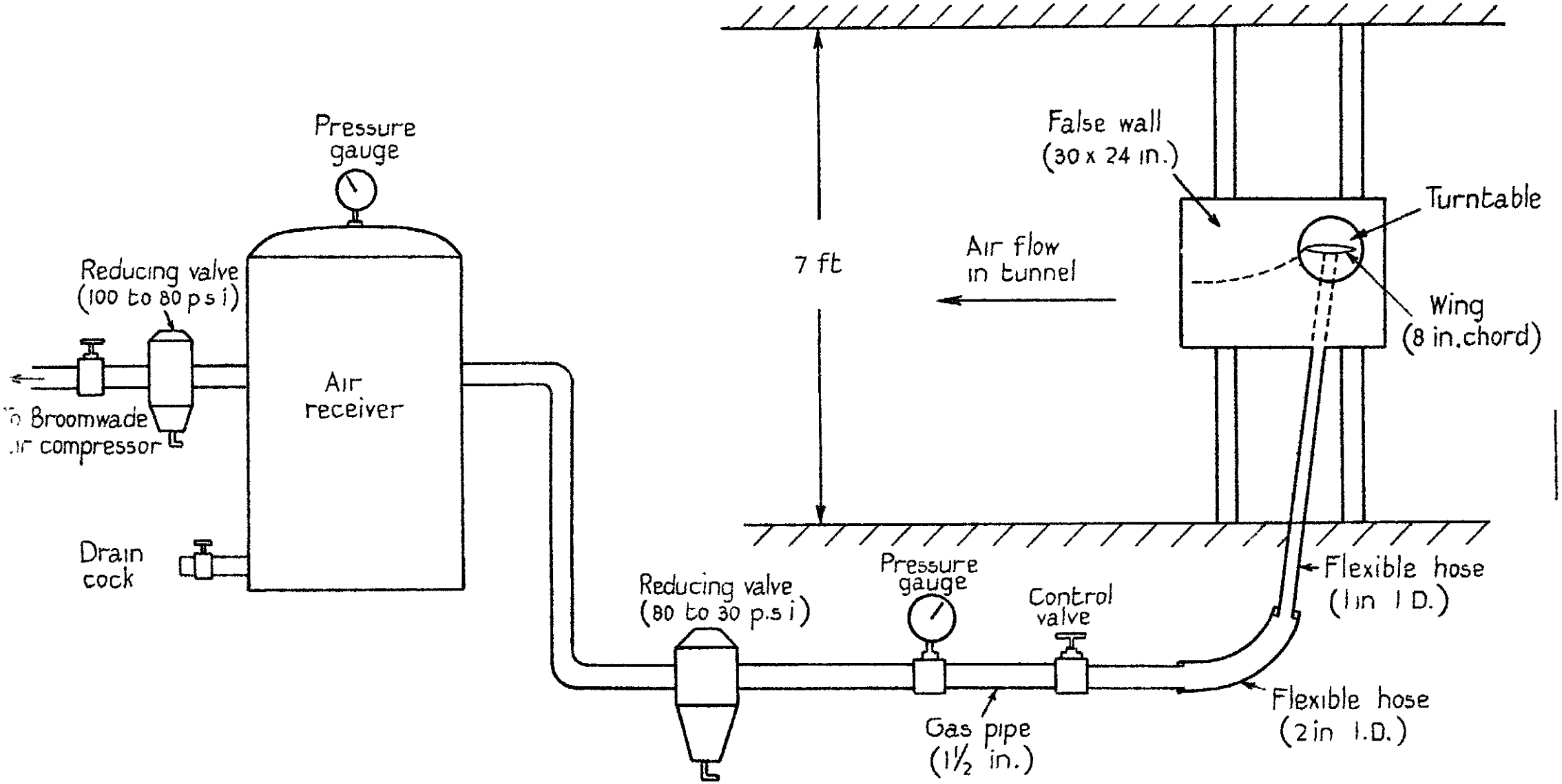

FIG. 1a.

Arrangement of jet flap model and external ducting

FIG. 1b.

Internal structure of three-dimensional jet flap model.

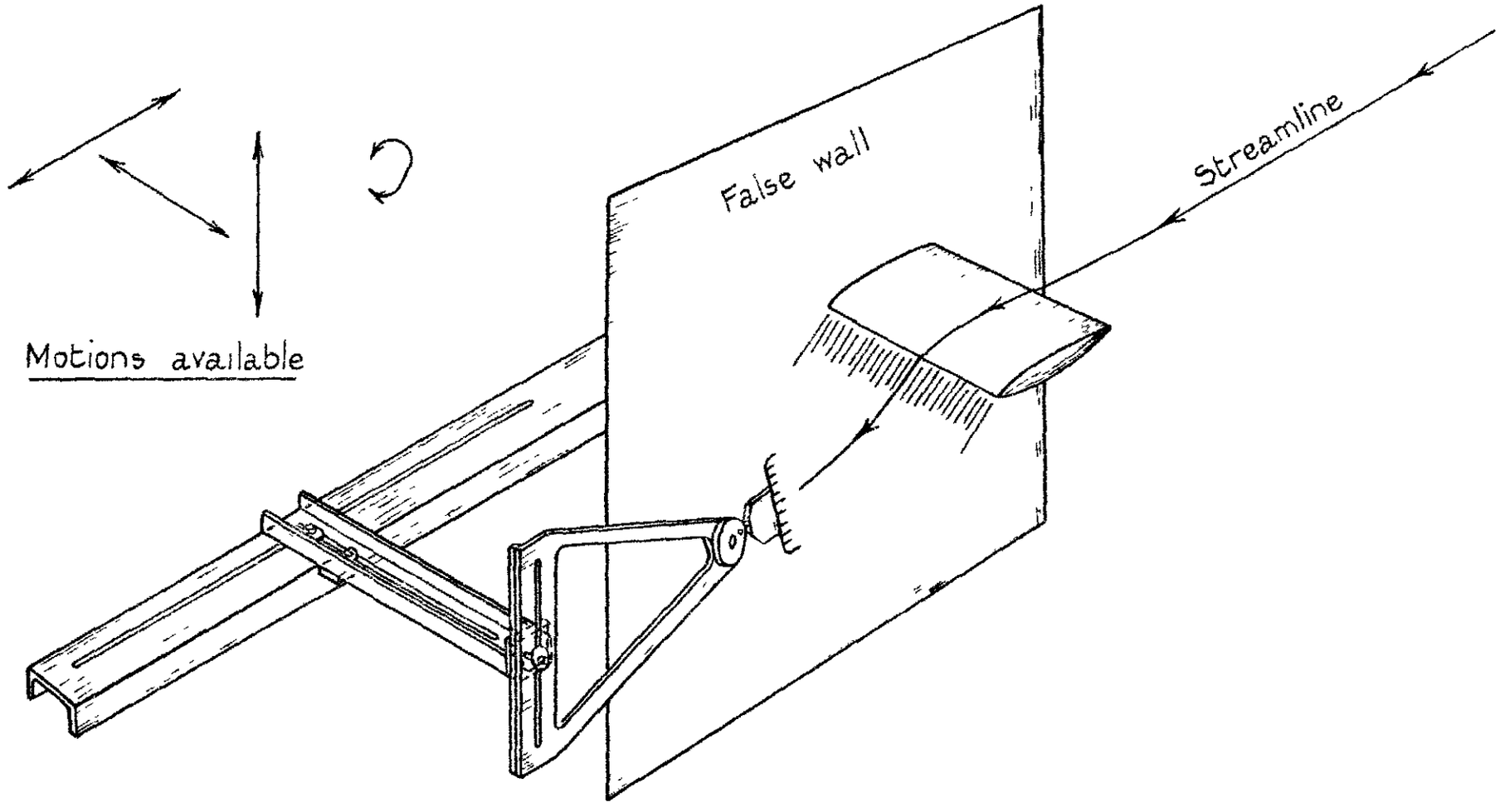

Scale : ≏ 1/10

Pitot comb wake traverse gear.

FIG. 1c

FIG. 2a.

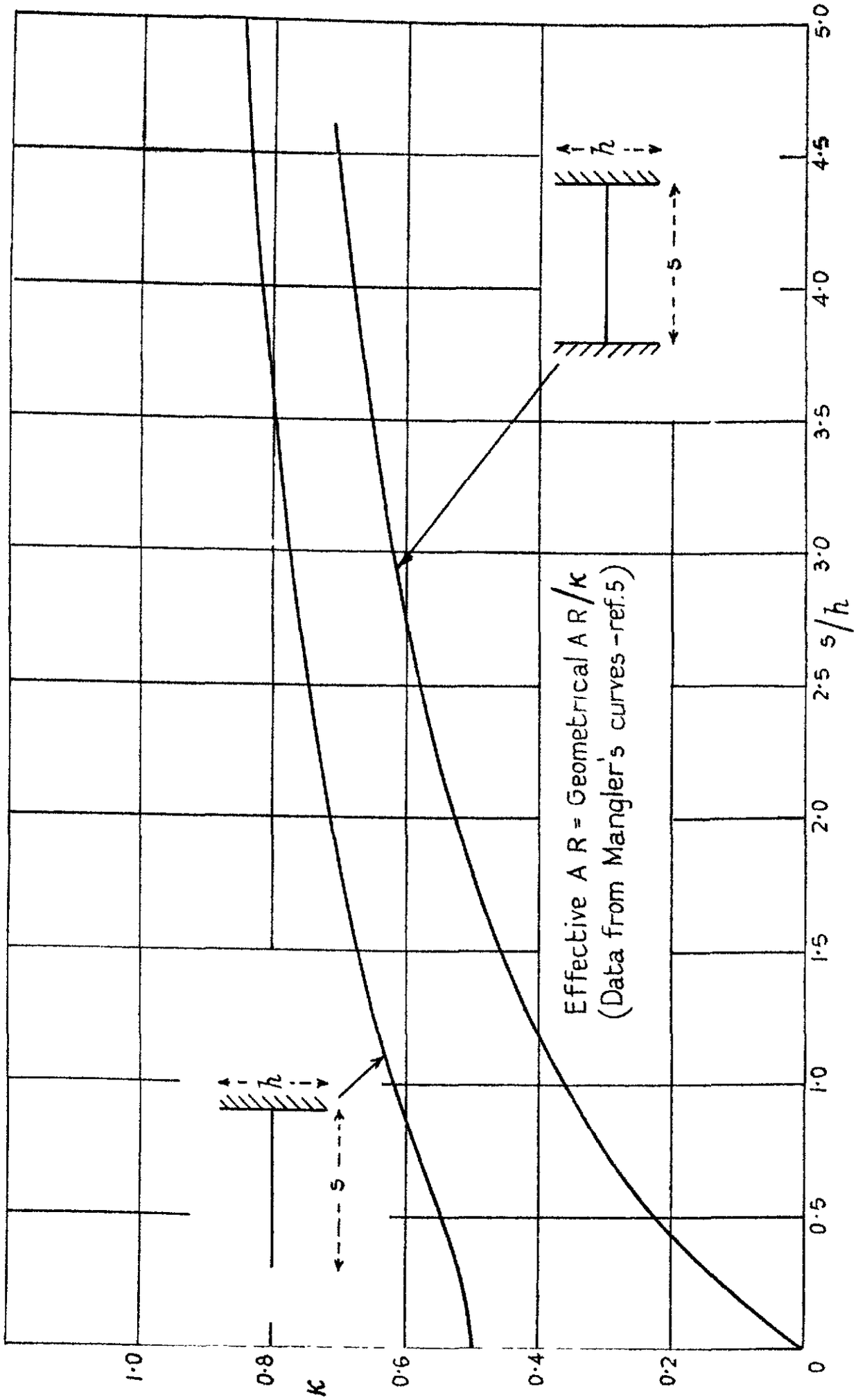

Variation of aspect ratio factor κ with ratio of wing span to end-plate height

Fig 2b.

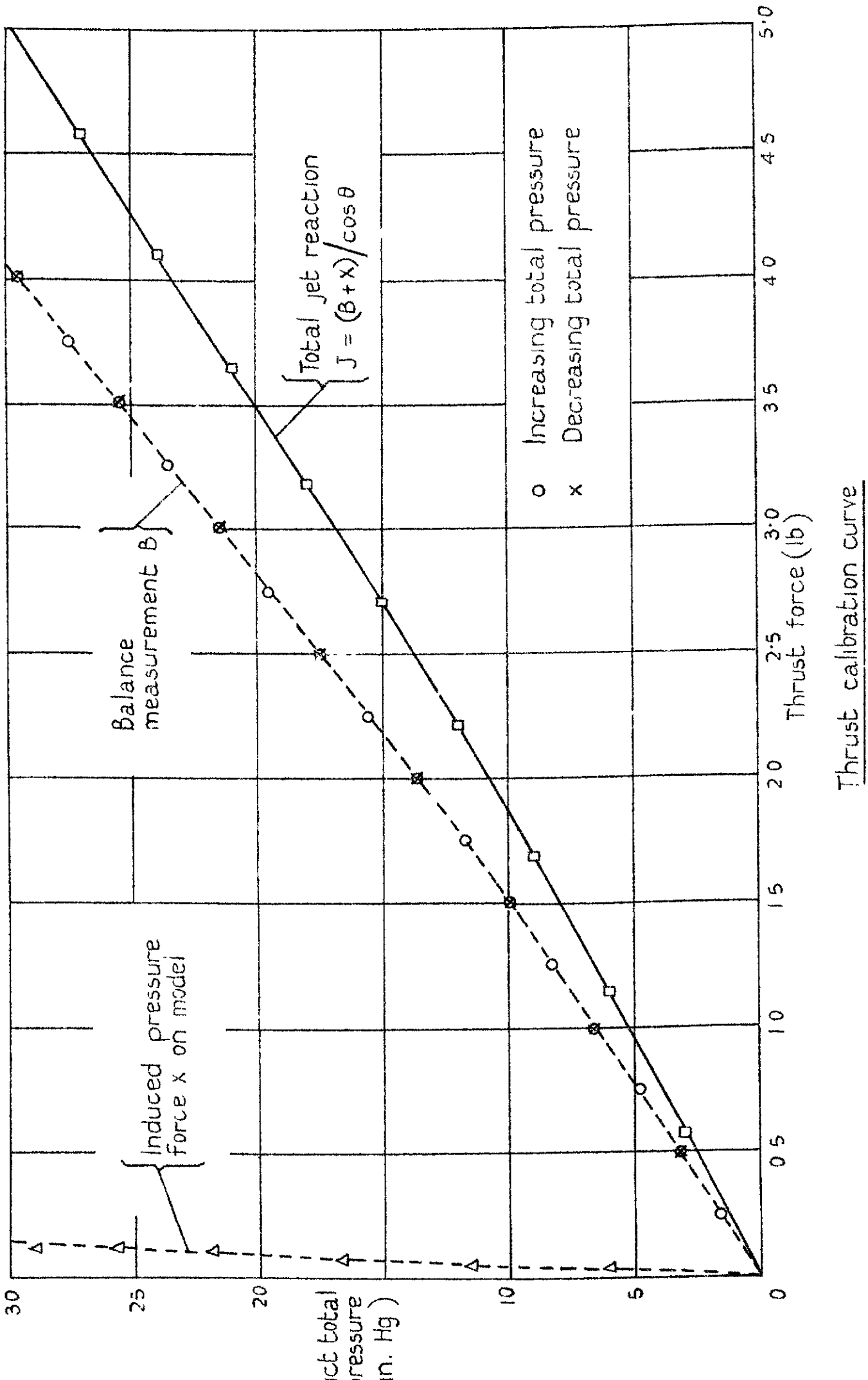

Thrust calibration curve

Fig 3a

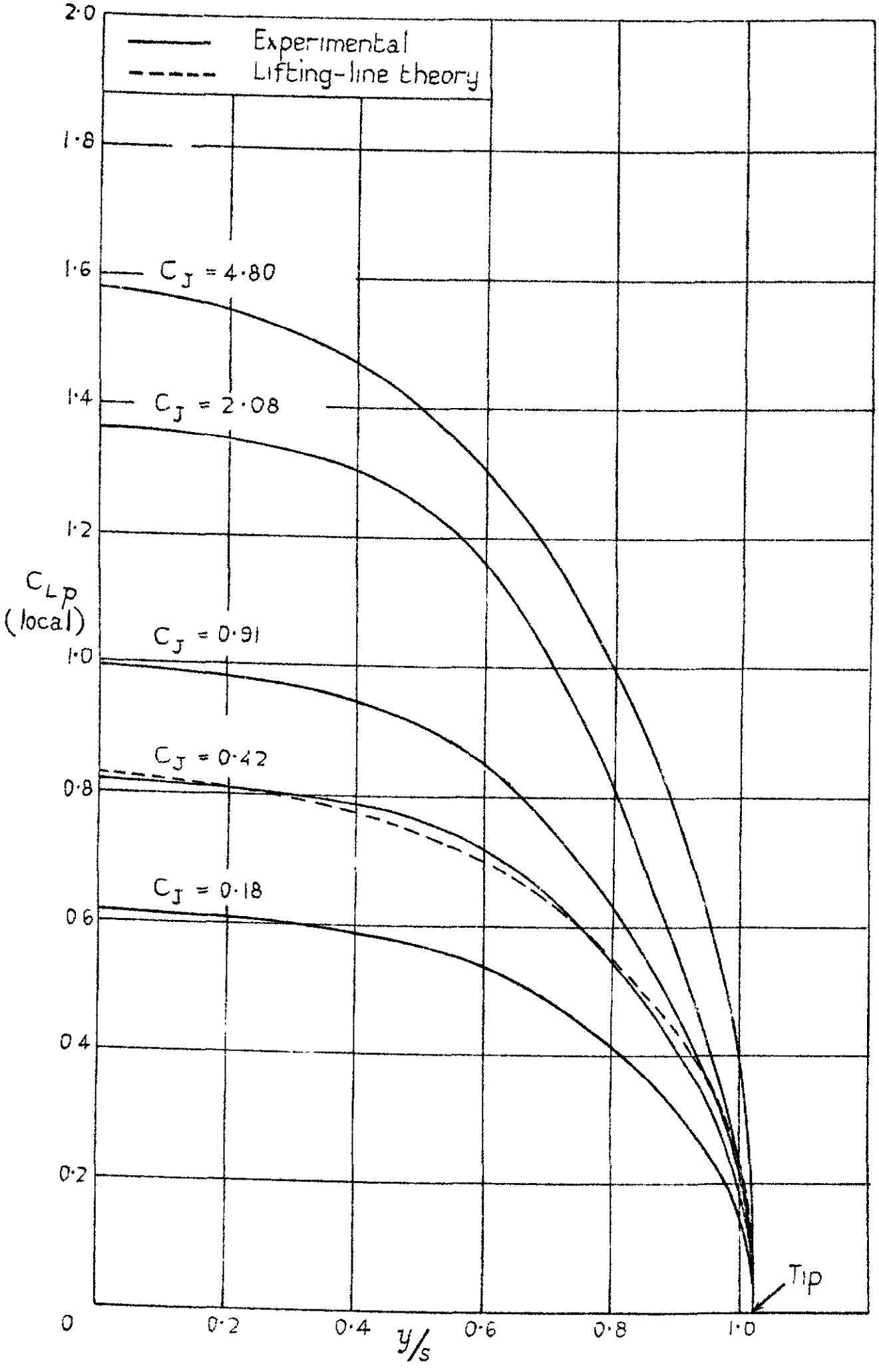

Spanwise distribution of pressure lift at zero incidence – Variation with C_J

Fig 3b.

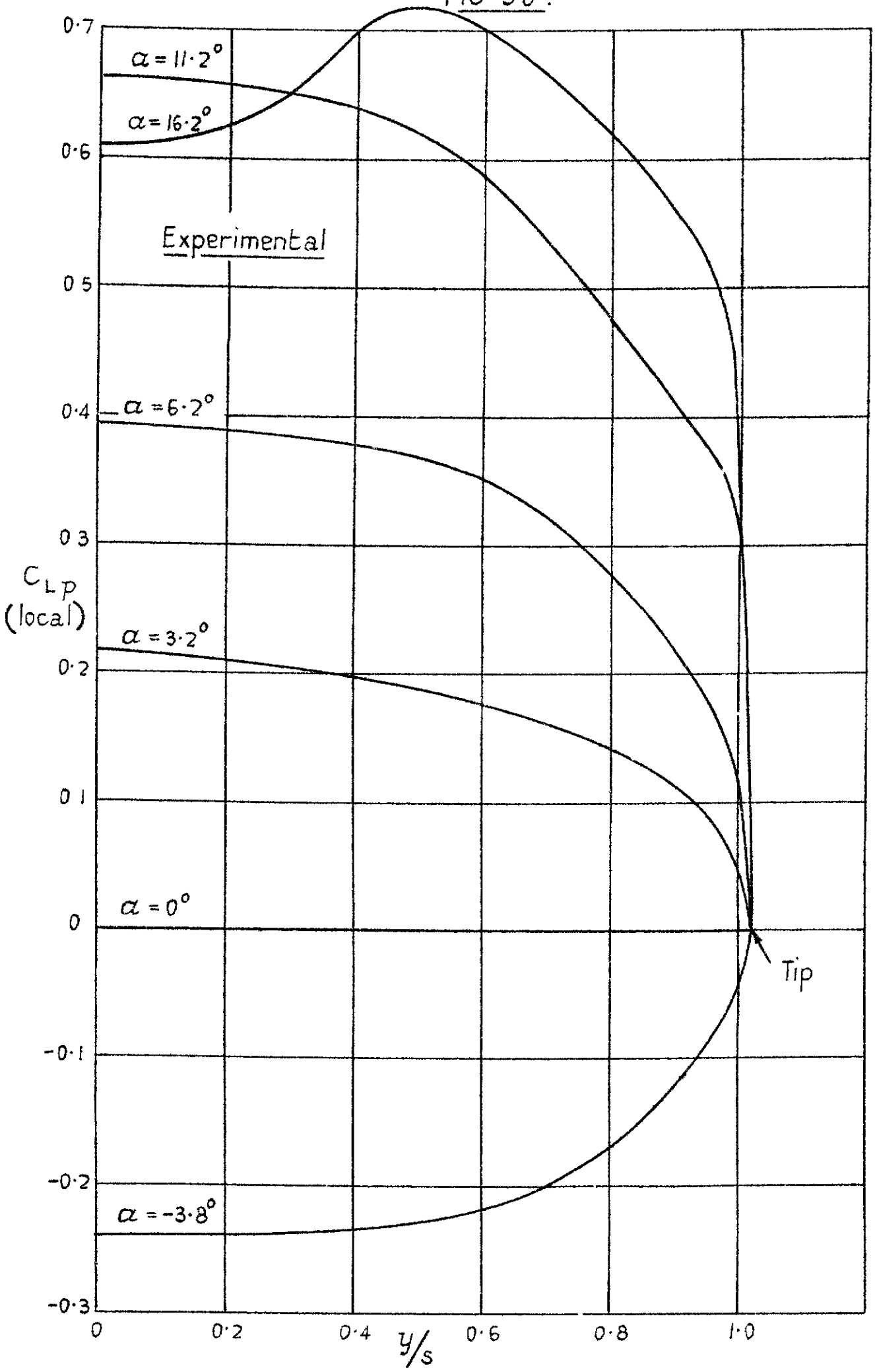

Spanwise distribution of lift without blowing.
Variation with incidence

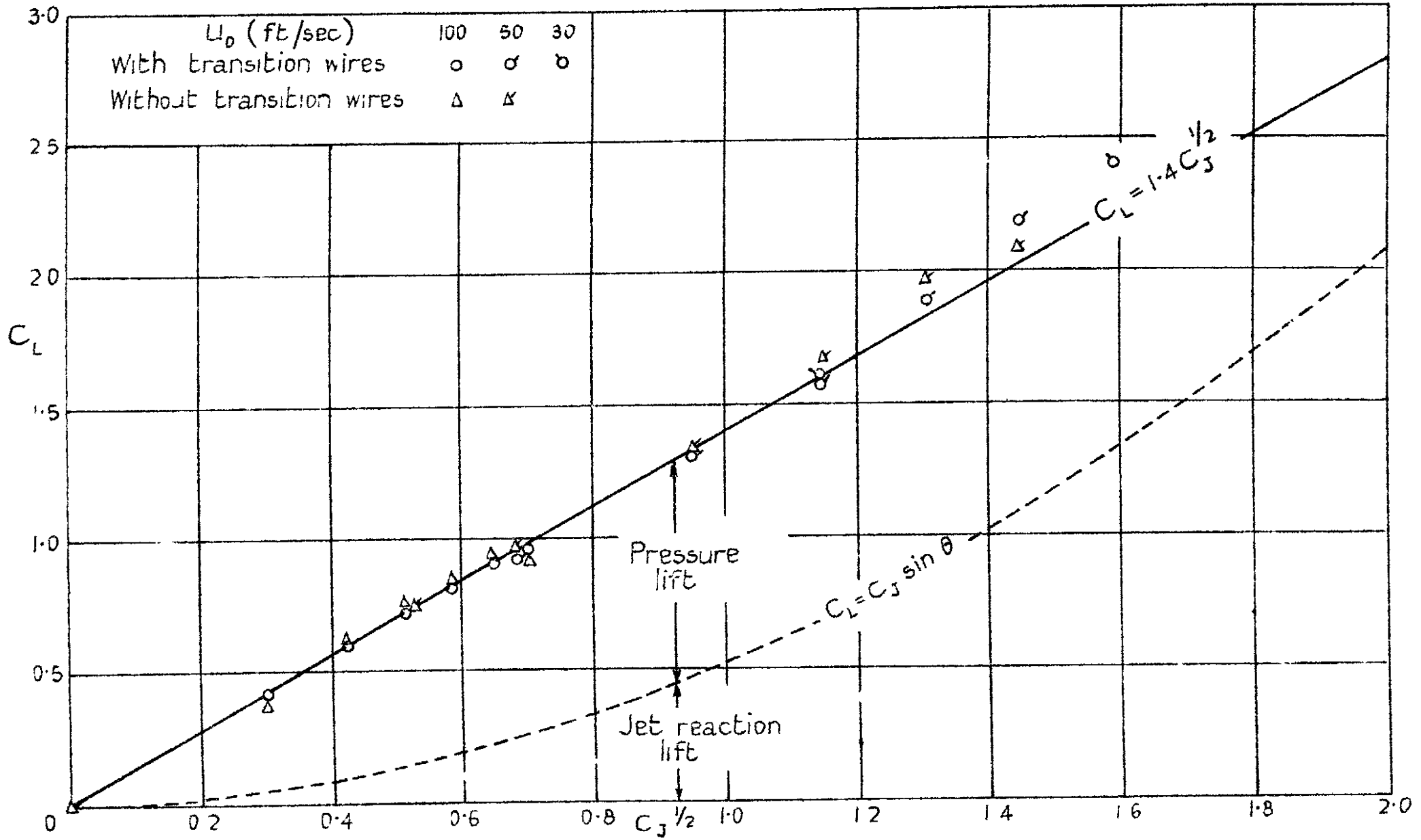

Variation of total lift C_L with $C_J^{1/2}$ at zero incidence

FIG 4a

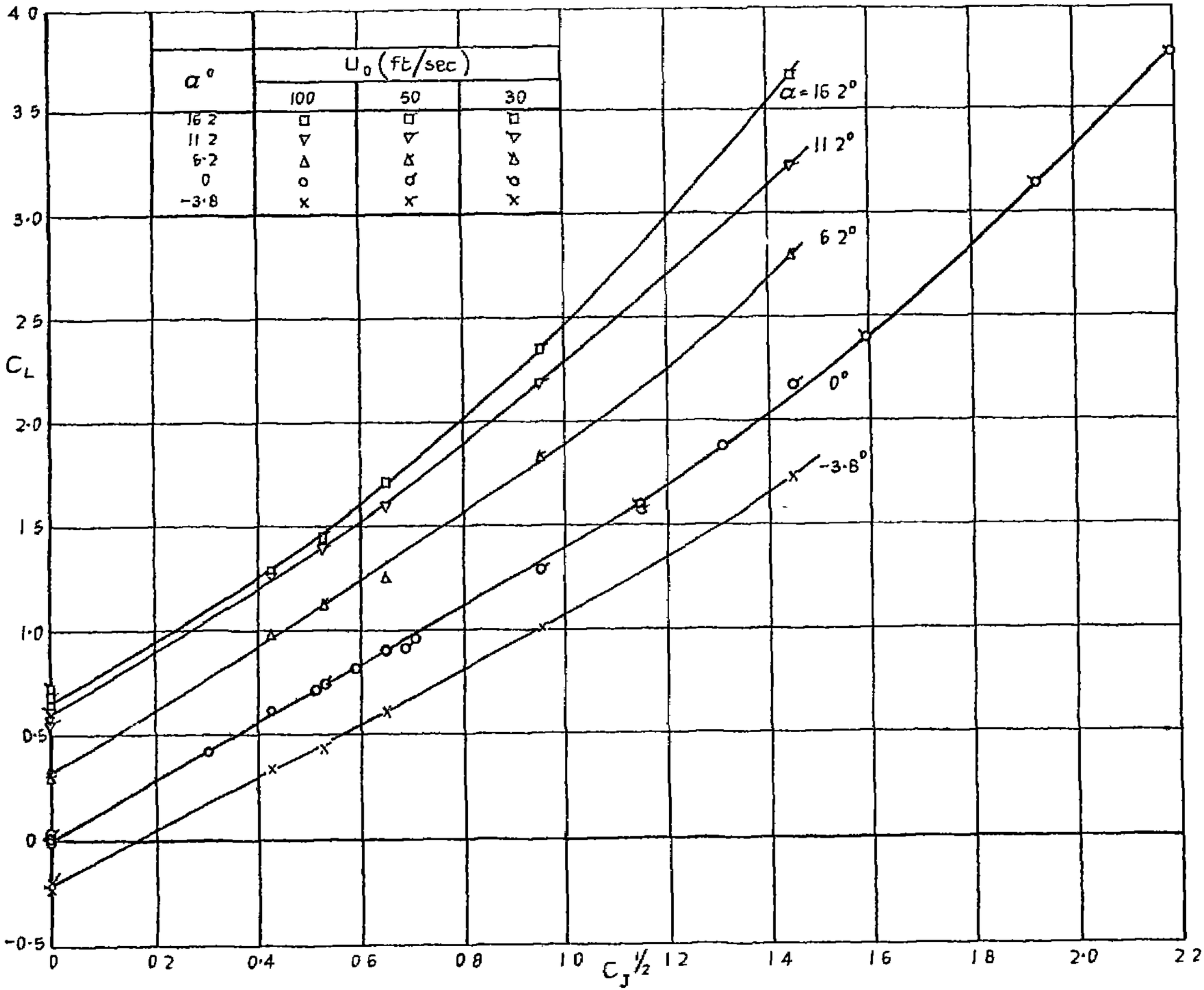

Variation of total lift with $C_J^{1/2}$ at constant incidence

FIG 5.

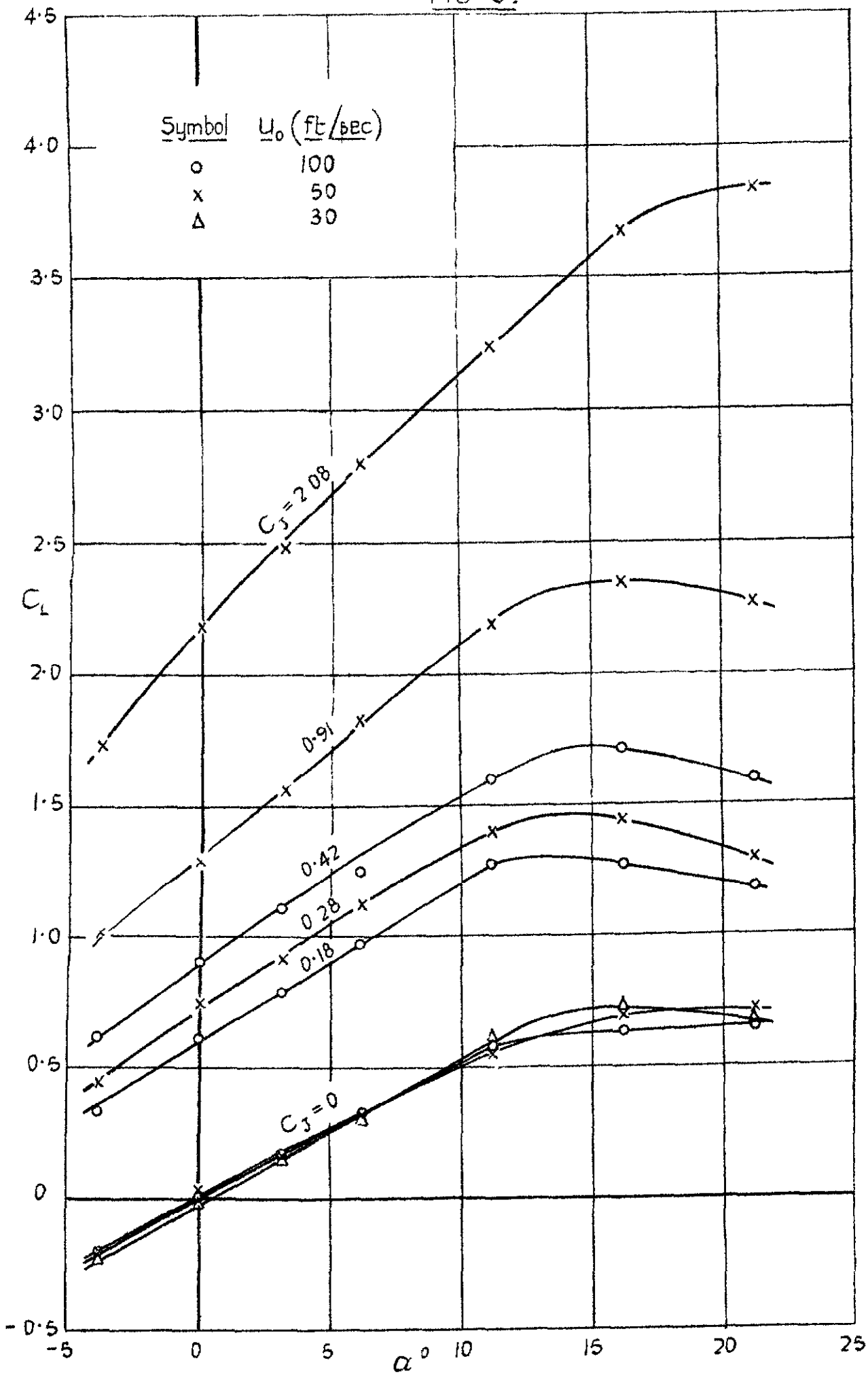

Variation of total lift with incidence at constant C_J

FIG. 6.

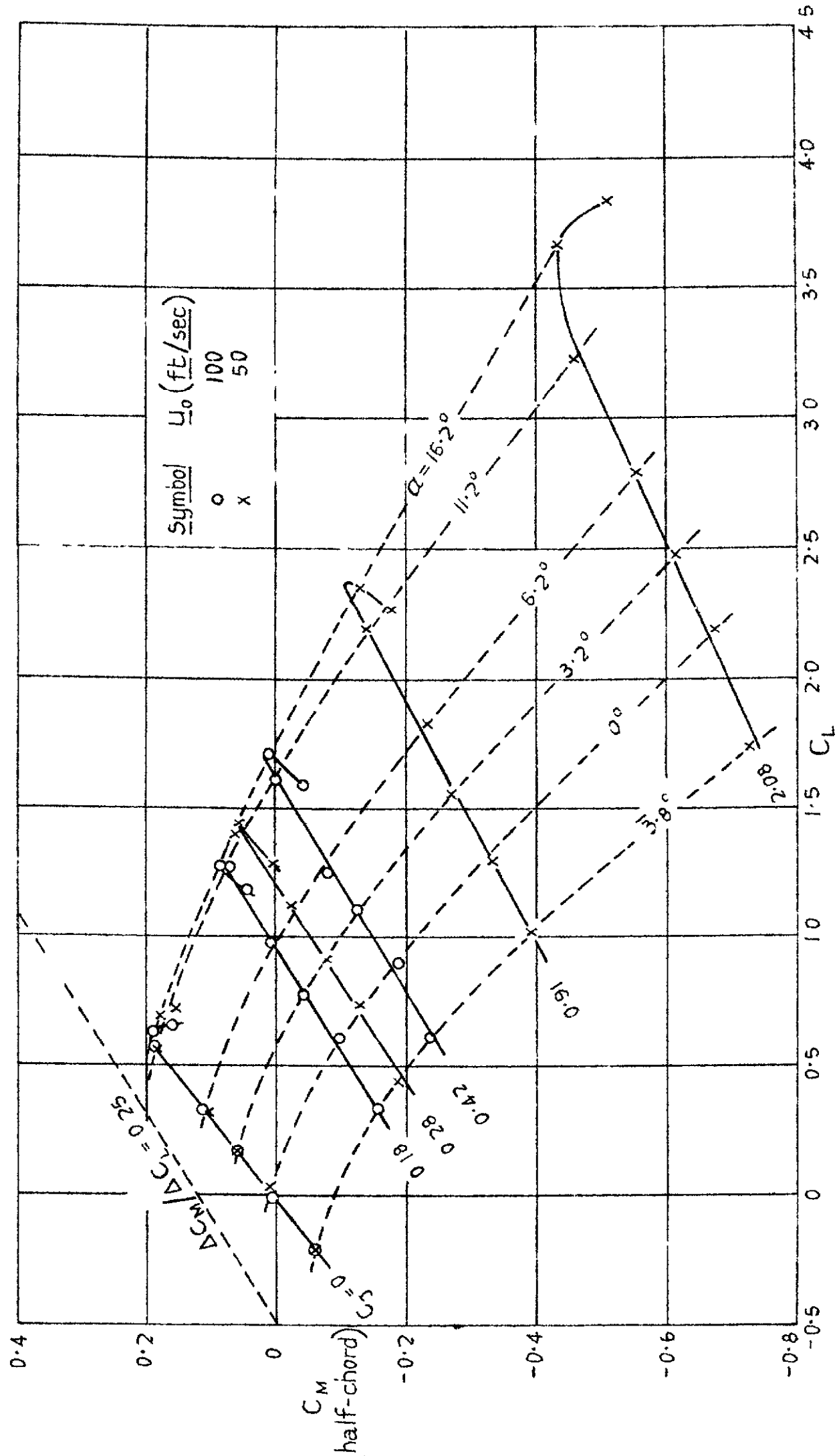

Variation of total pitching moment with total lift.

FIG. 7.

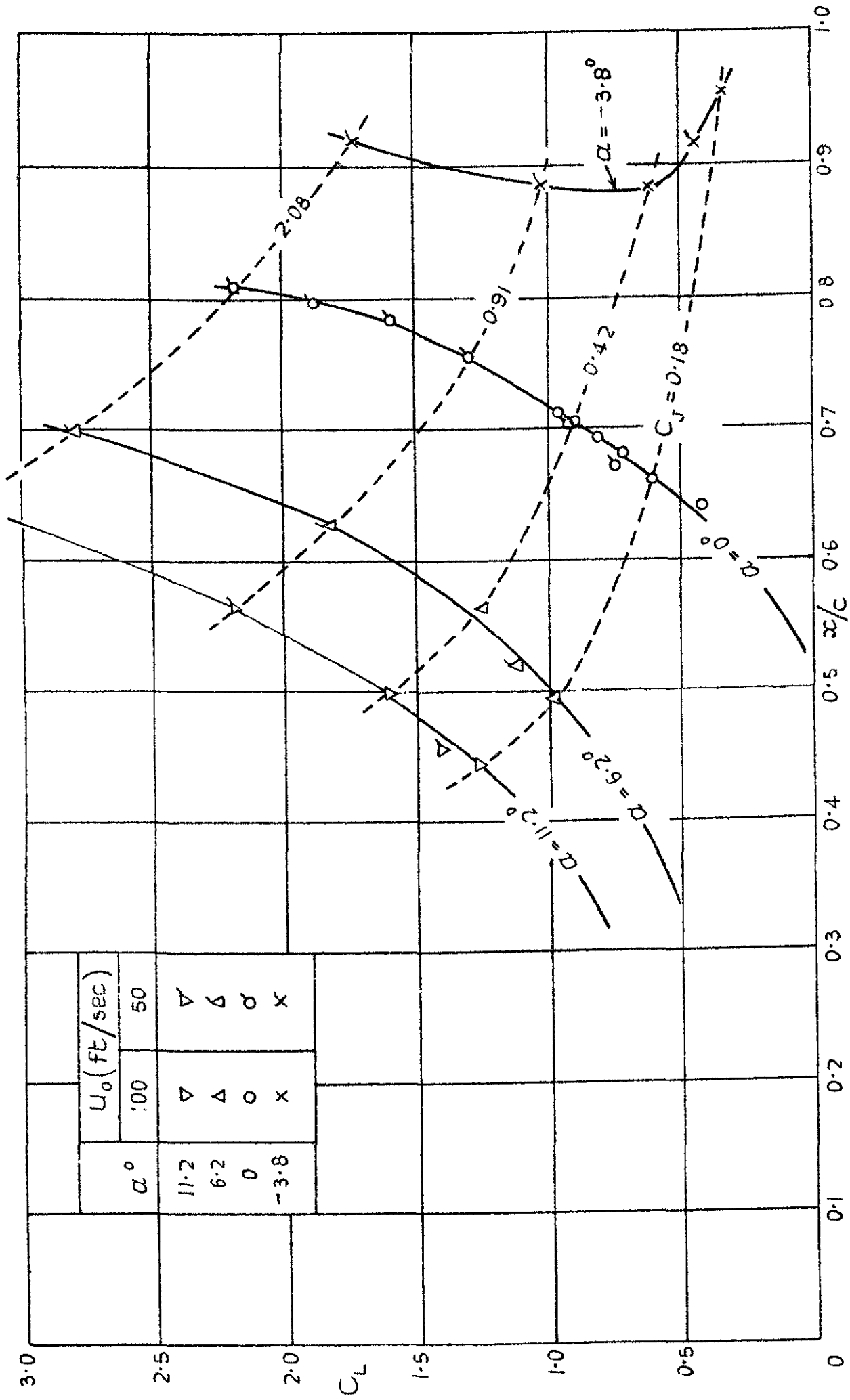

Variation in position of centre of total lift.

FIG. 8a.

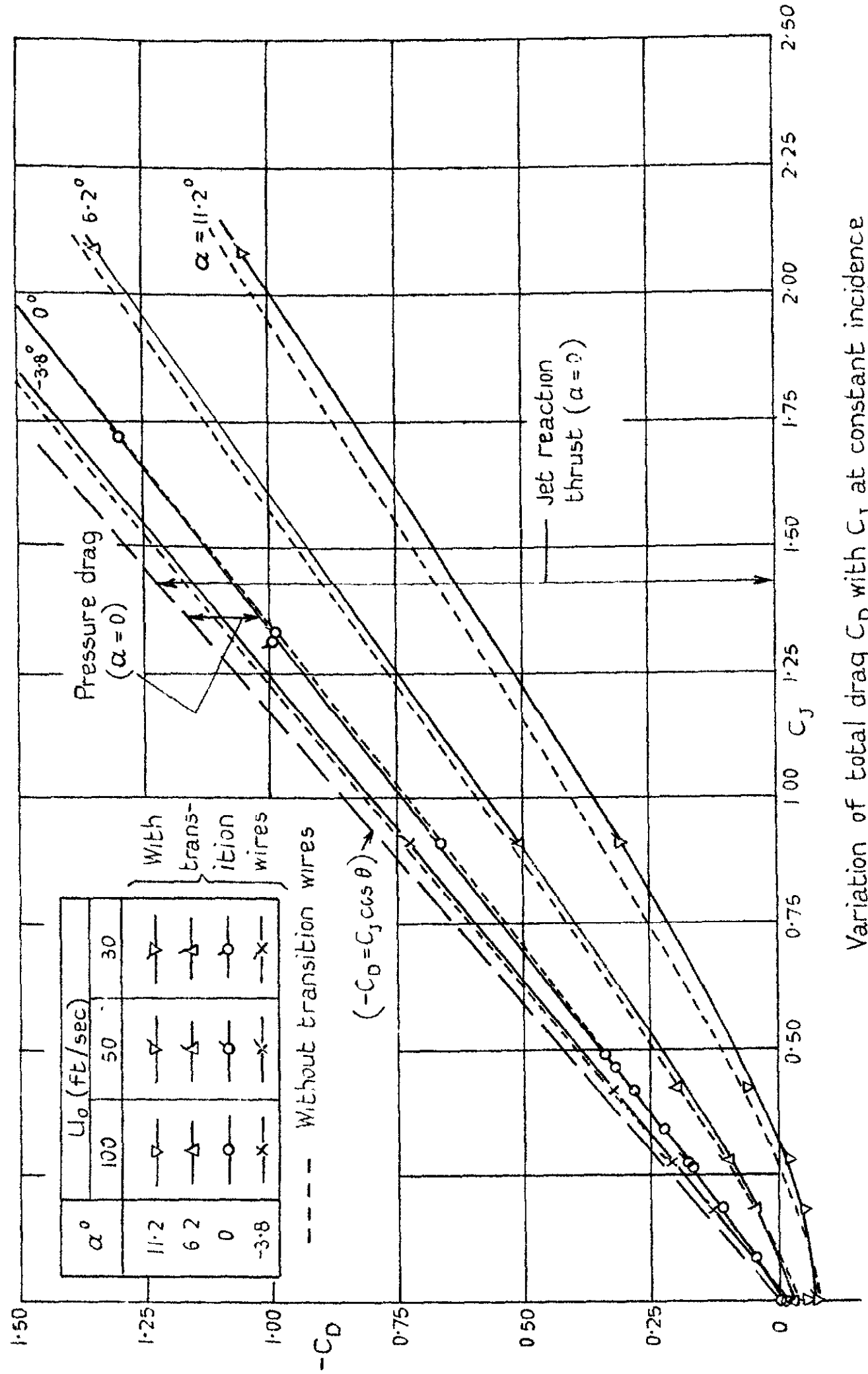

Variation of total drag C_D with C_J at constant incidence

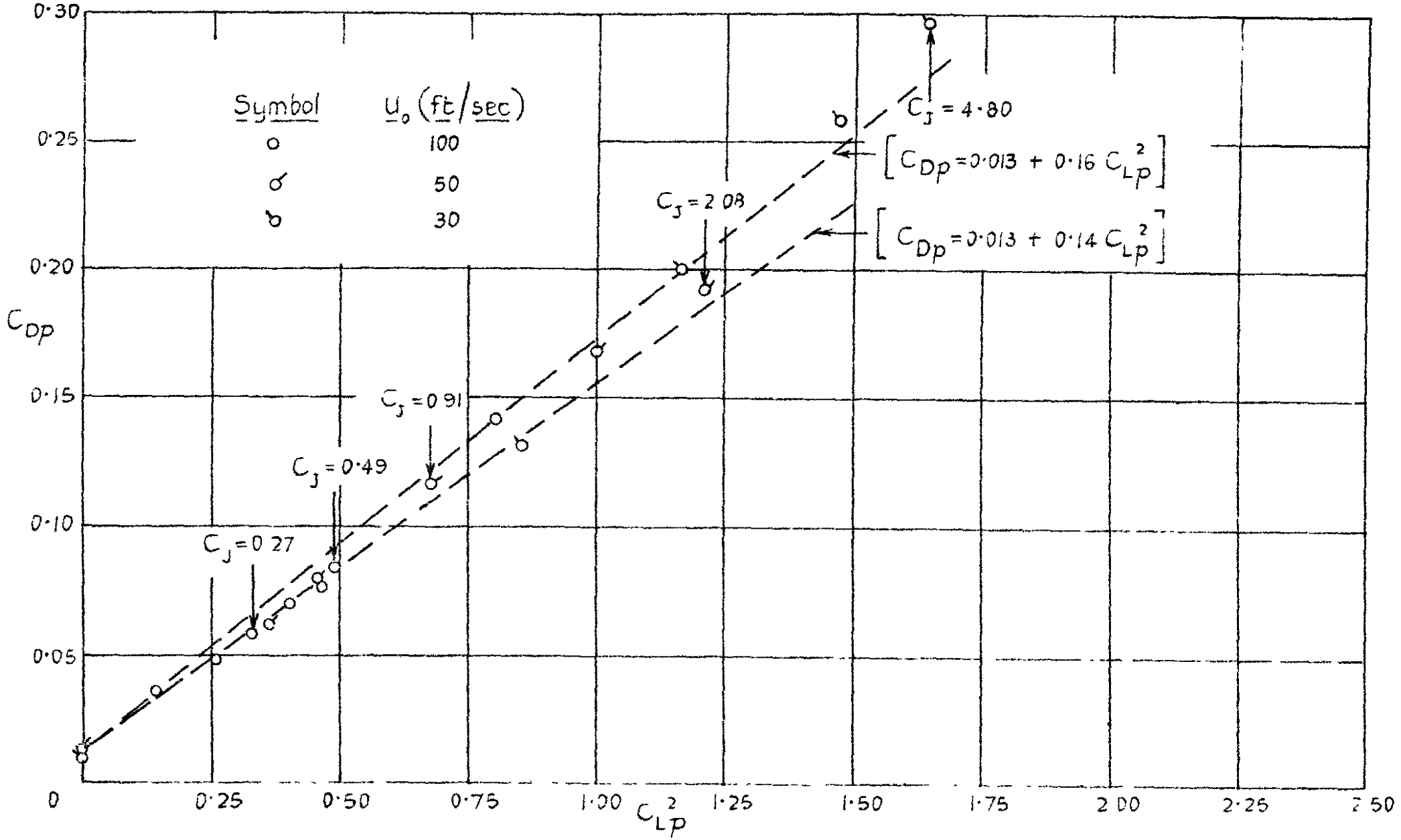

FIG. 8b.

Variation of pressure drag C_{Dp} with C_{Lp}^2 at zero incidence.

FIG. 8c.

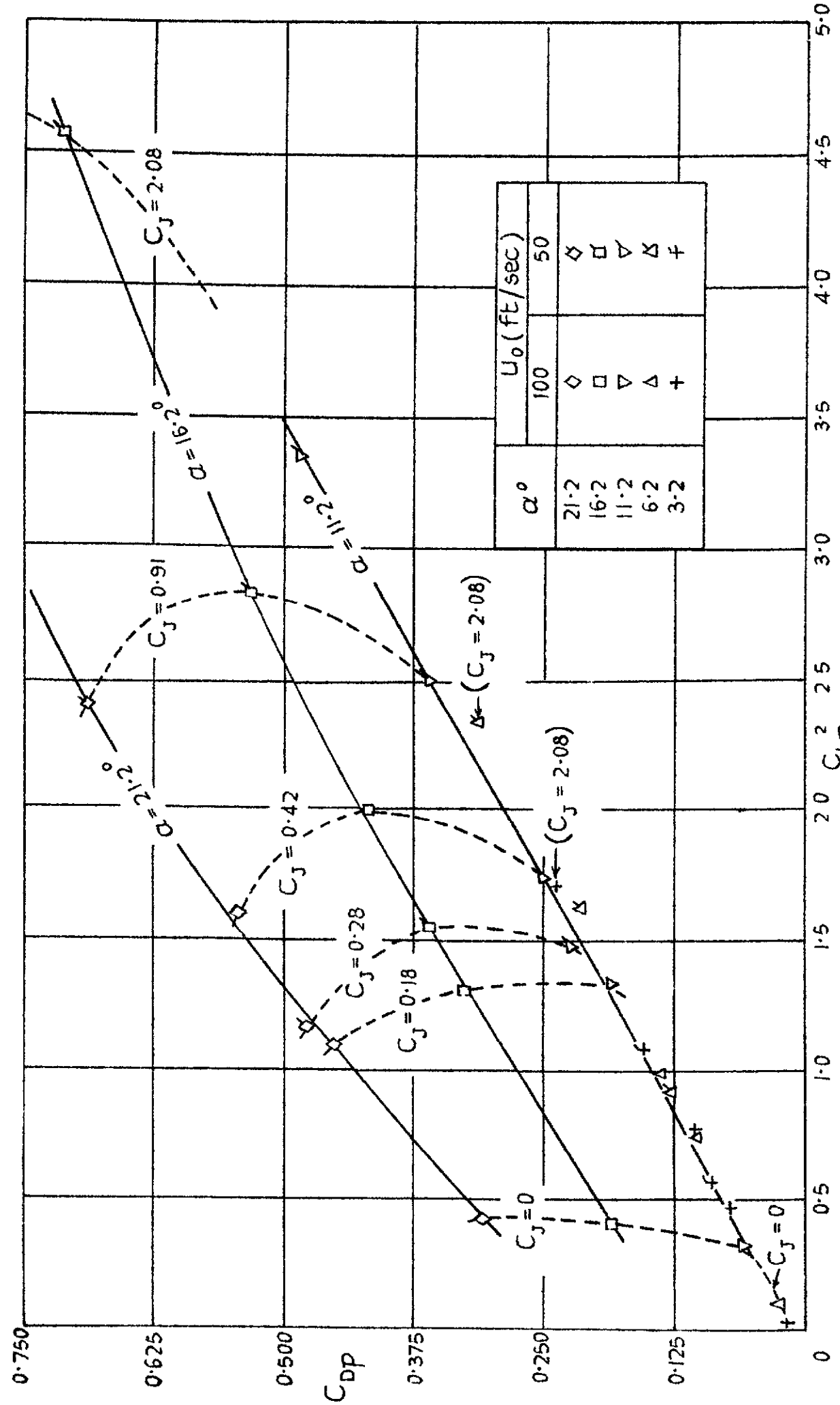

Variation of pressure drag C_{Dp} with C_{Lp}^2.

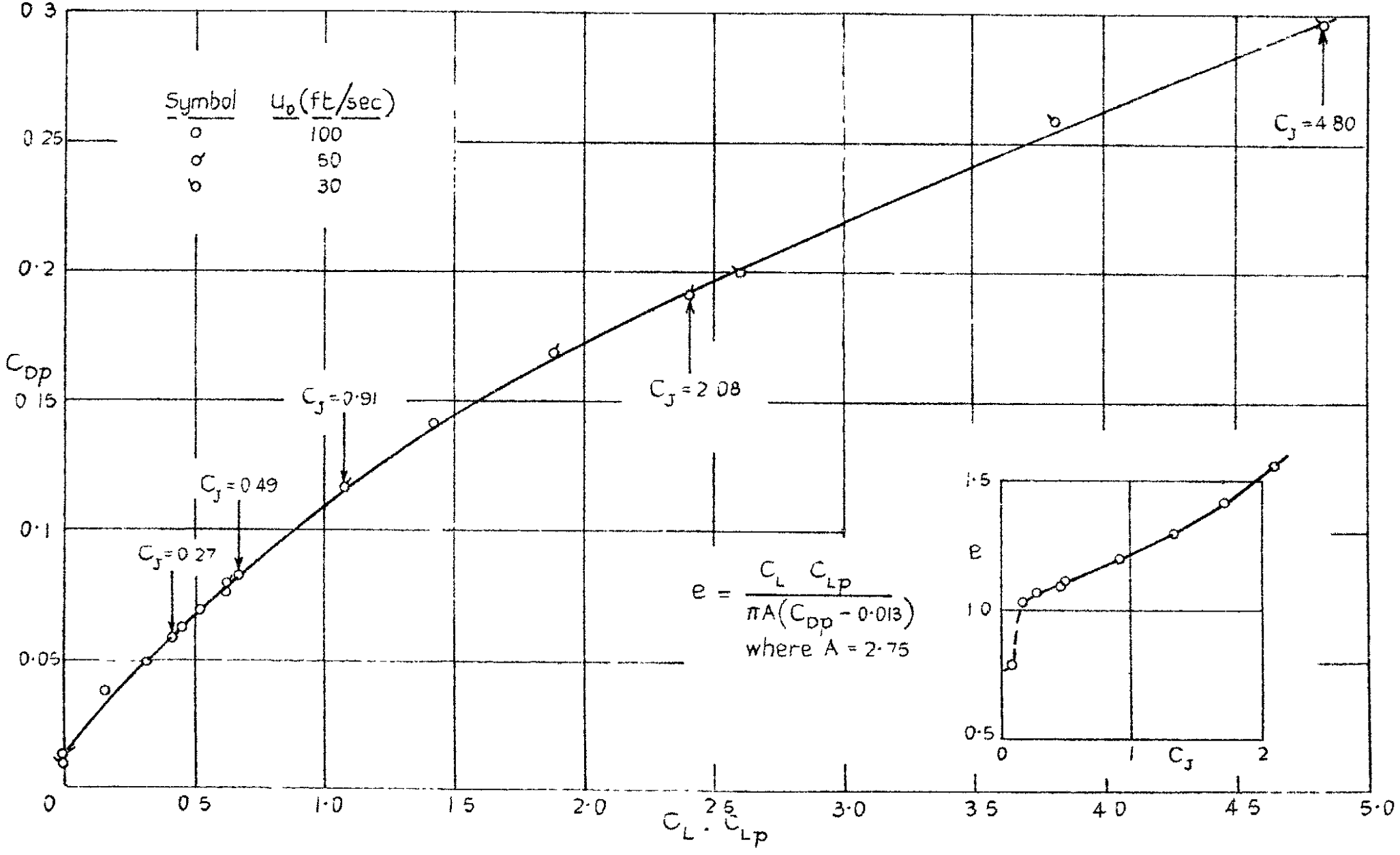

Fig 68

Variation of pressure drag C_{Dp} with $C_L \cdot C_{Lp}$ at zero incidence

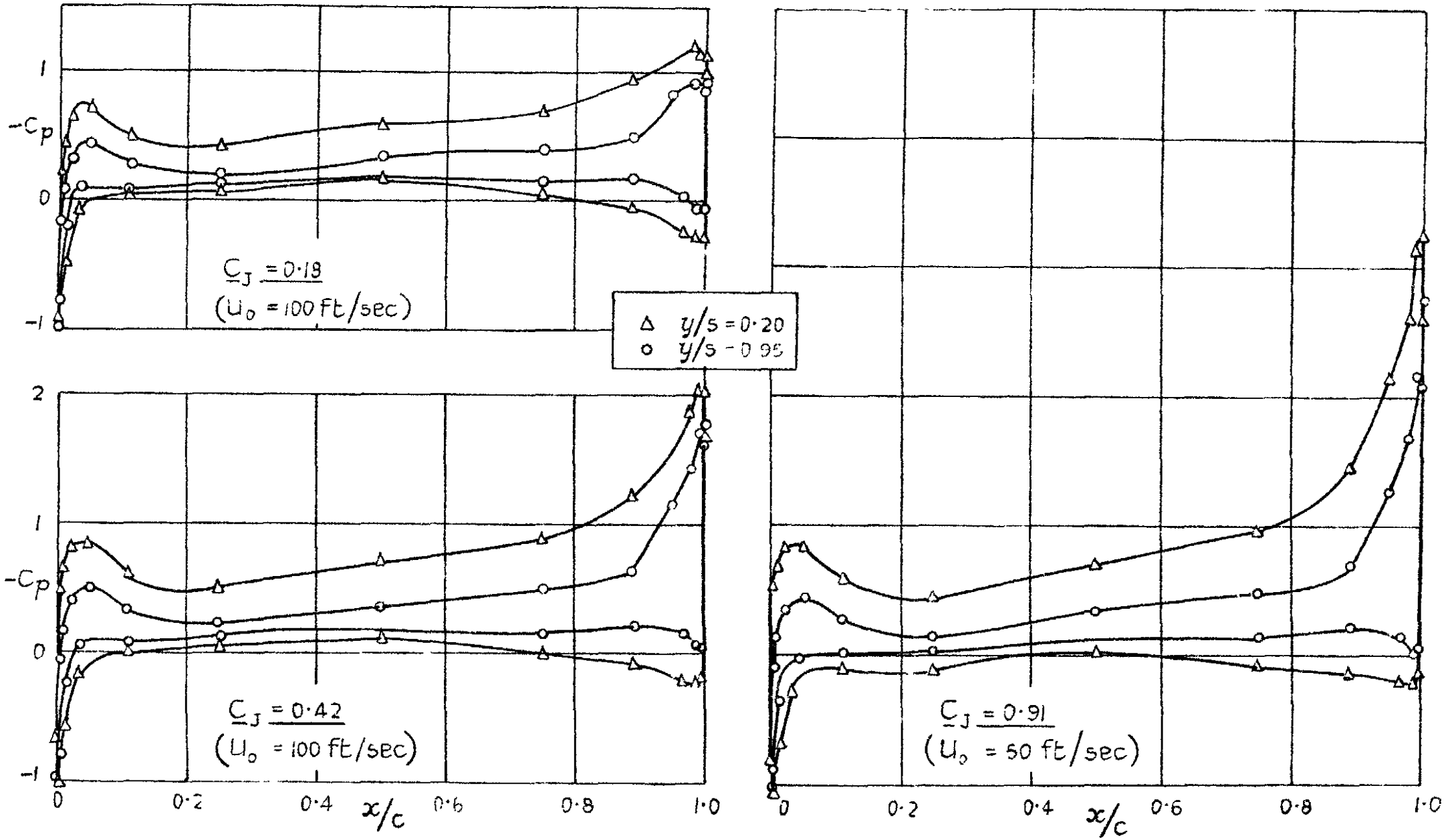

Fig 9.2

Chordwise pressure distributions at zero incidence Variation with C_J

Fig 9b

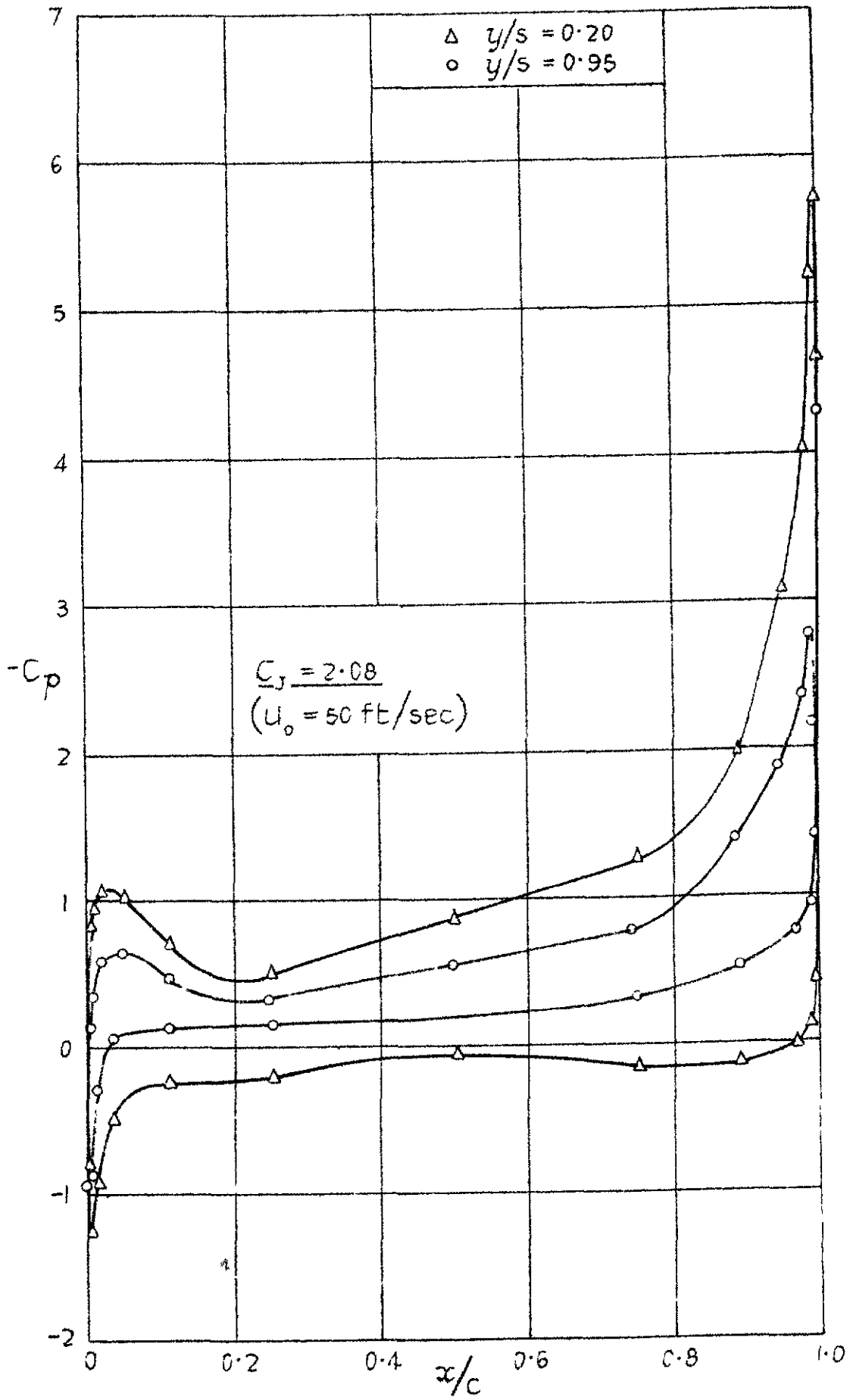

Chordwise pressure distributions at zero incidence
Variation with C_J.

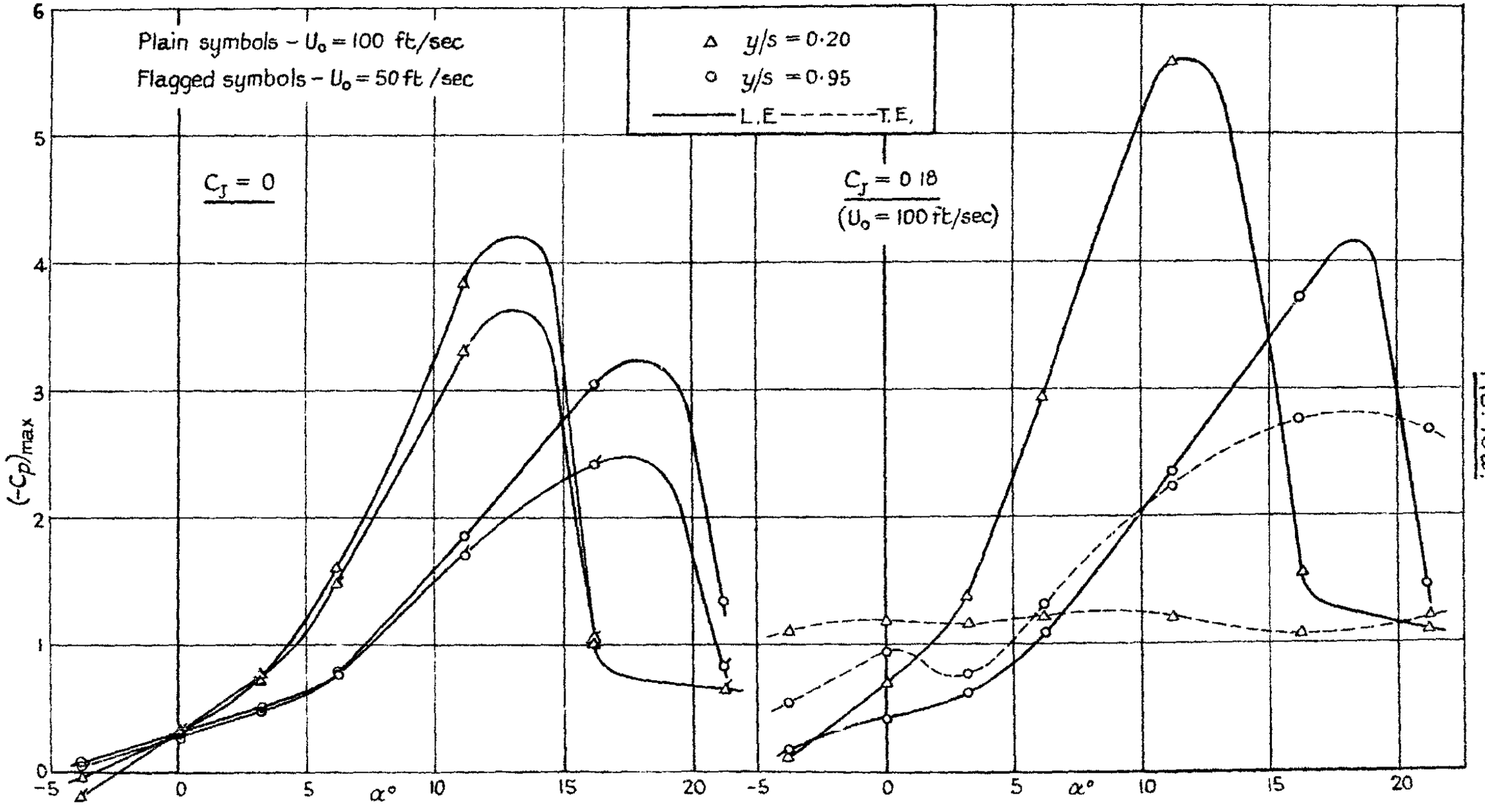

Variation of peak suctions near L E and T.E.

FIG. 10a.

FIG. 10 c

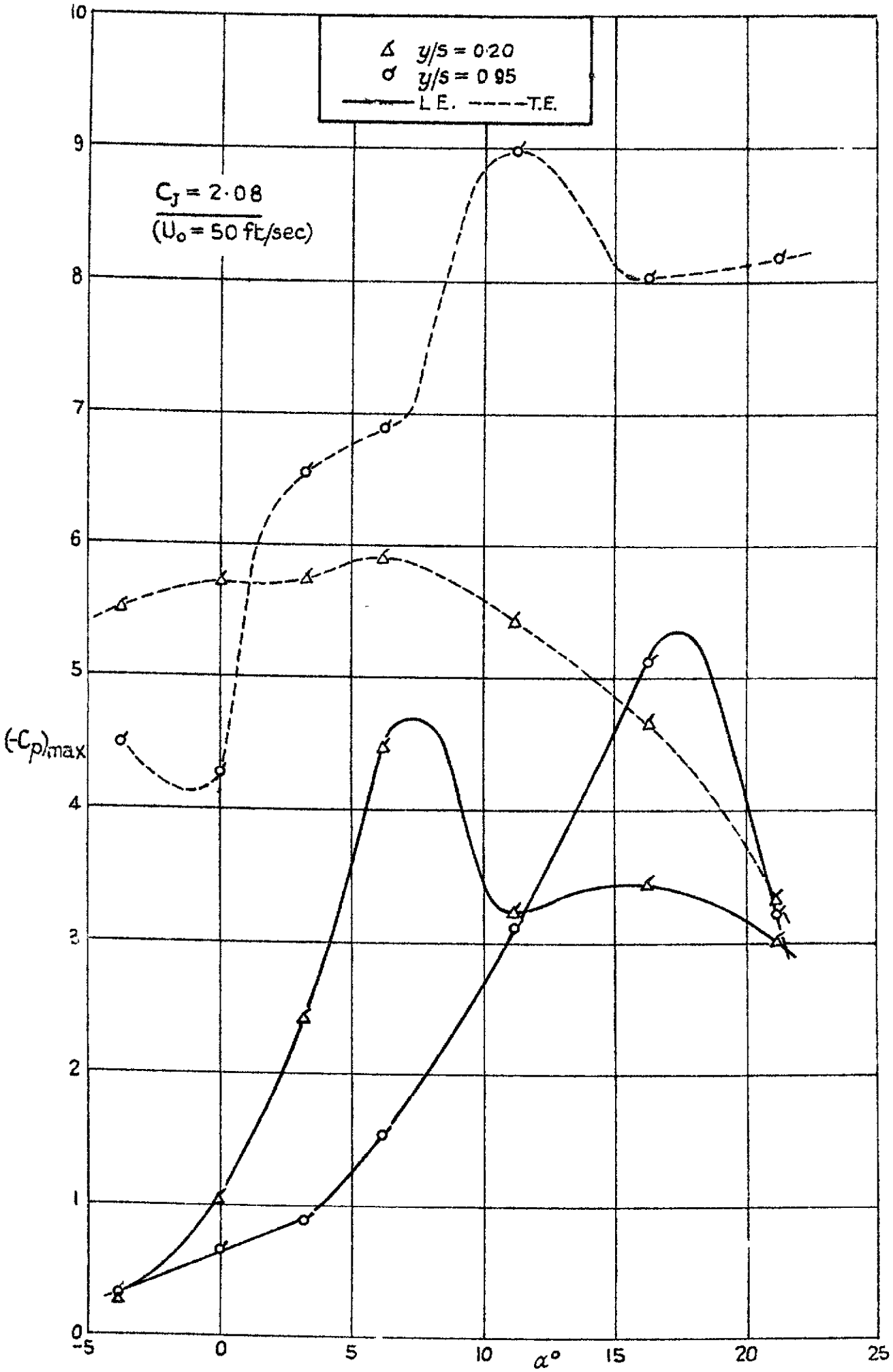

Variation of peak suctions near L.E and T.E

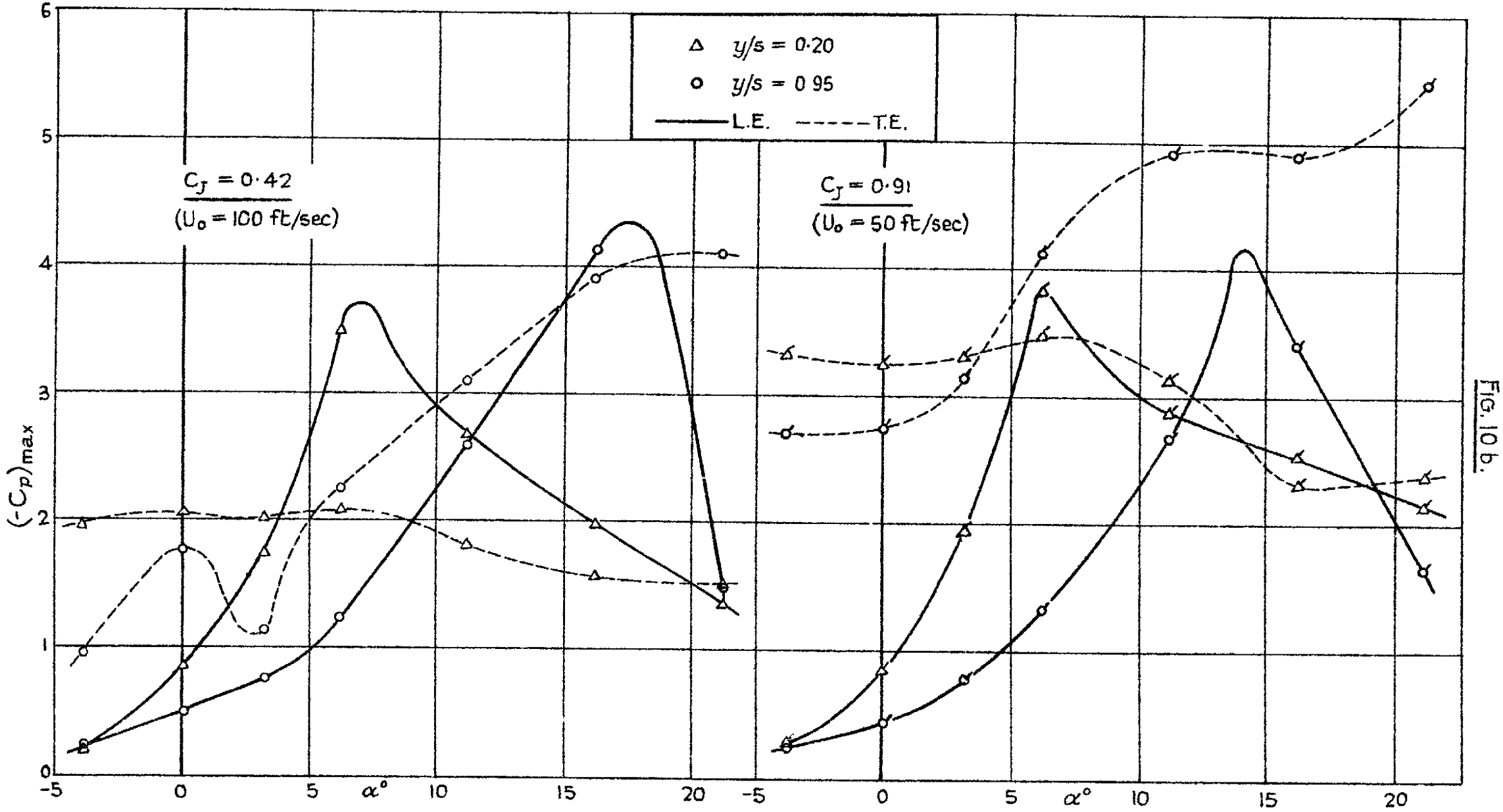

Fig. 10 b.

Variation of peak suctions near L.E. and T.E

FIG. 10 c

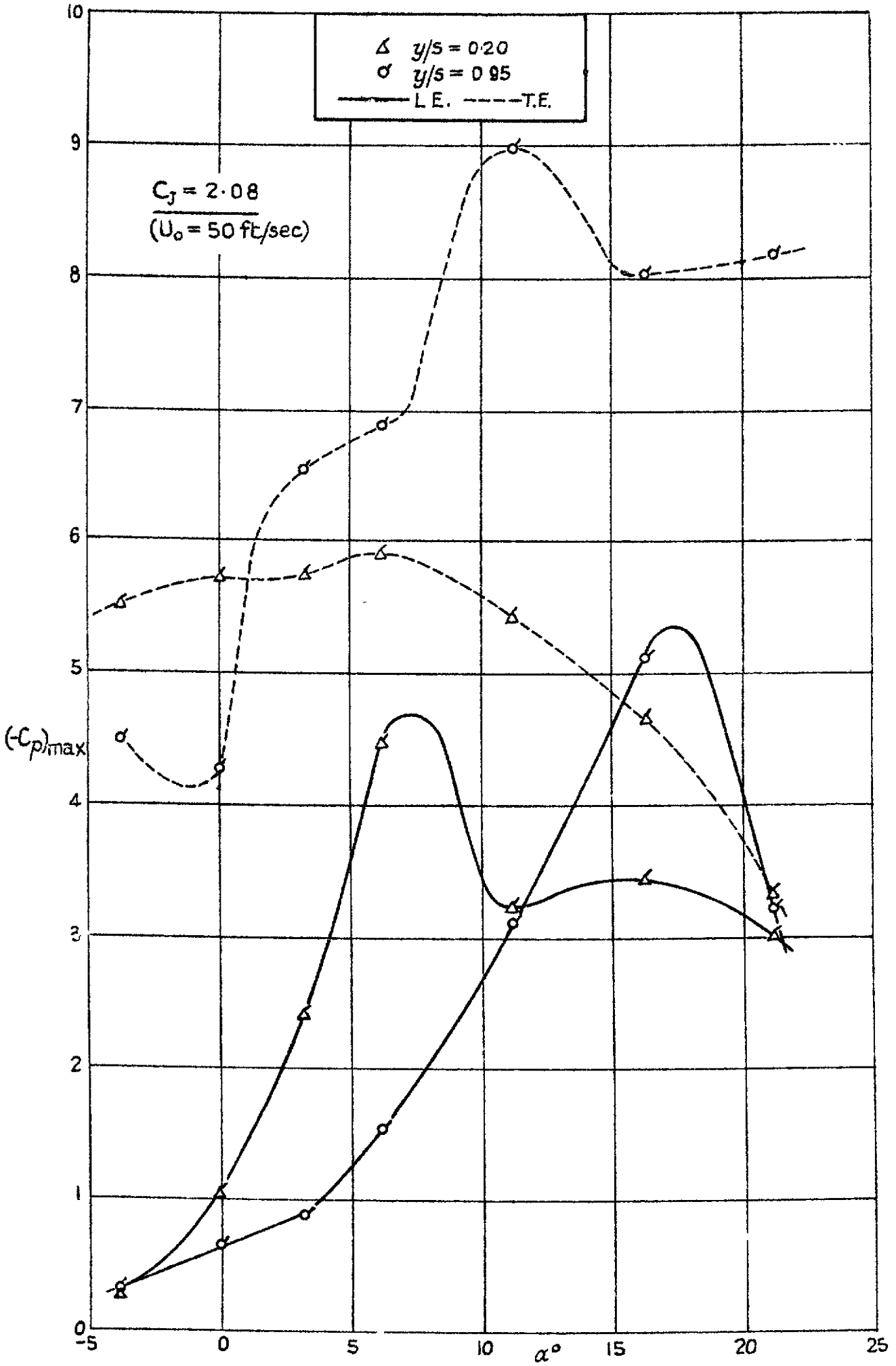

Variation of peak suctions near L.E. and T.E

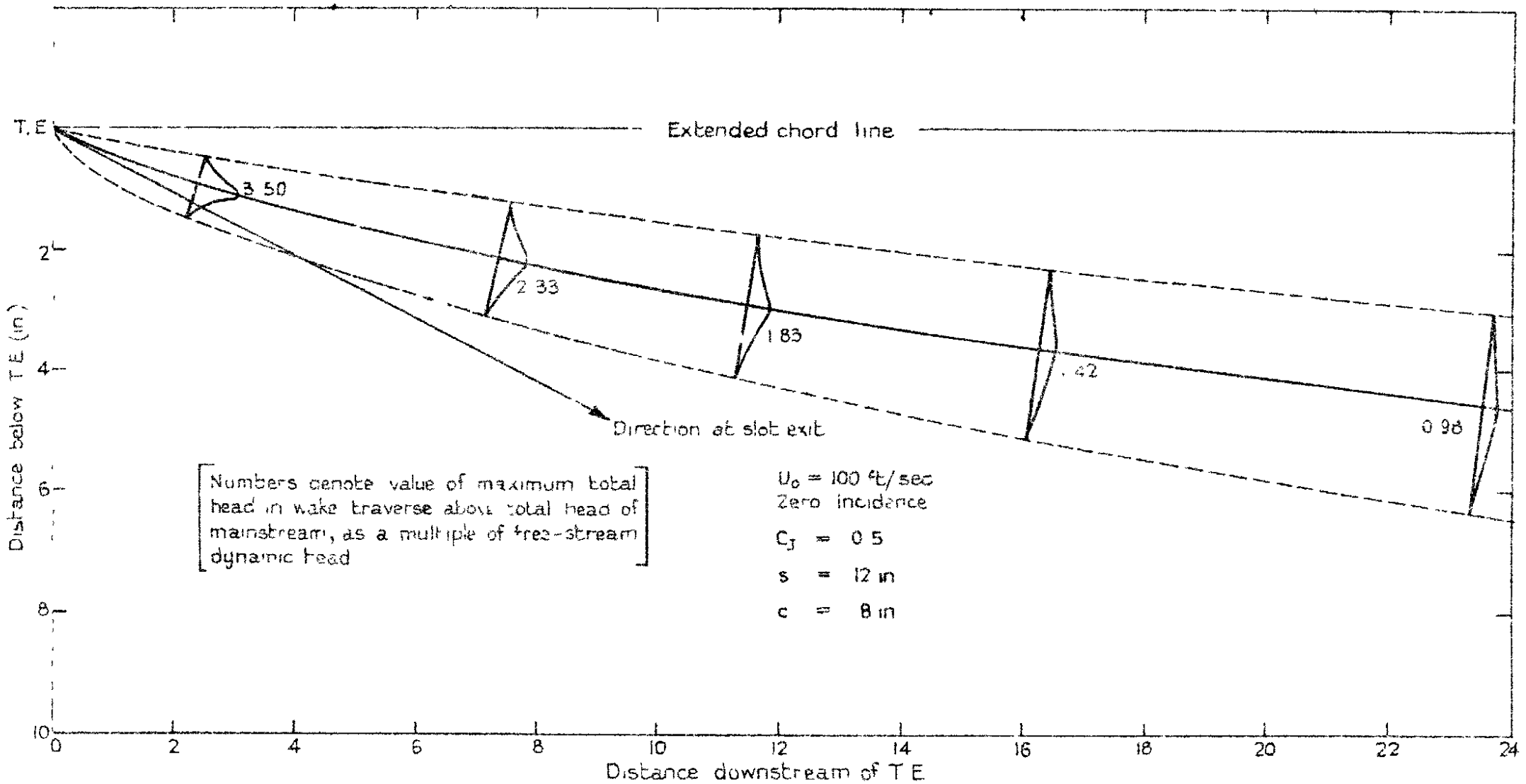

Fig 11a

Mean line and total head profiles of jet at mid-span position

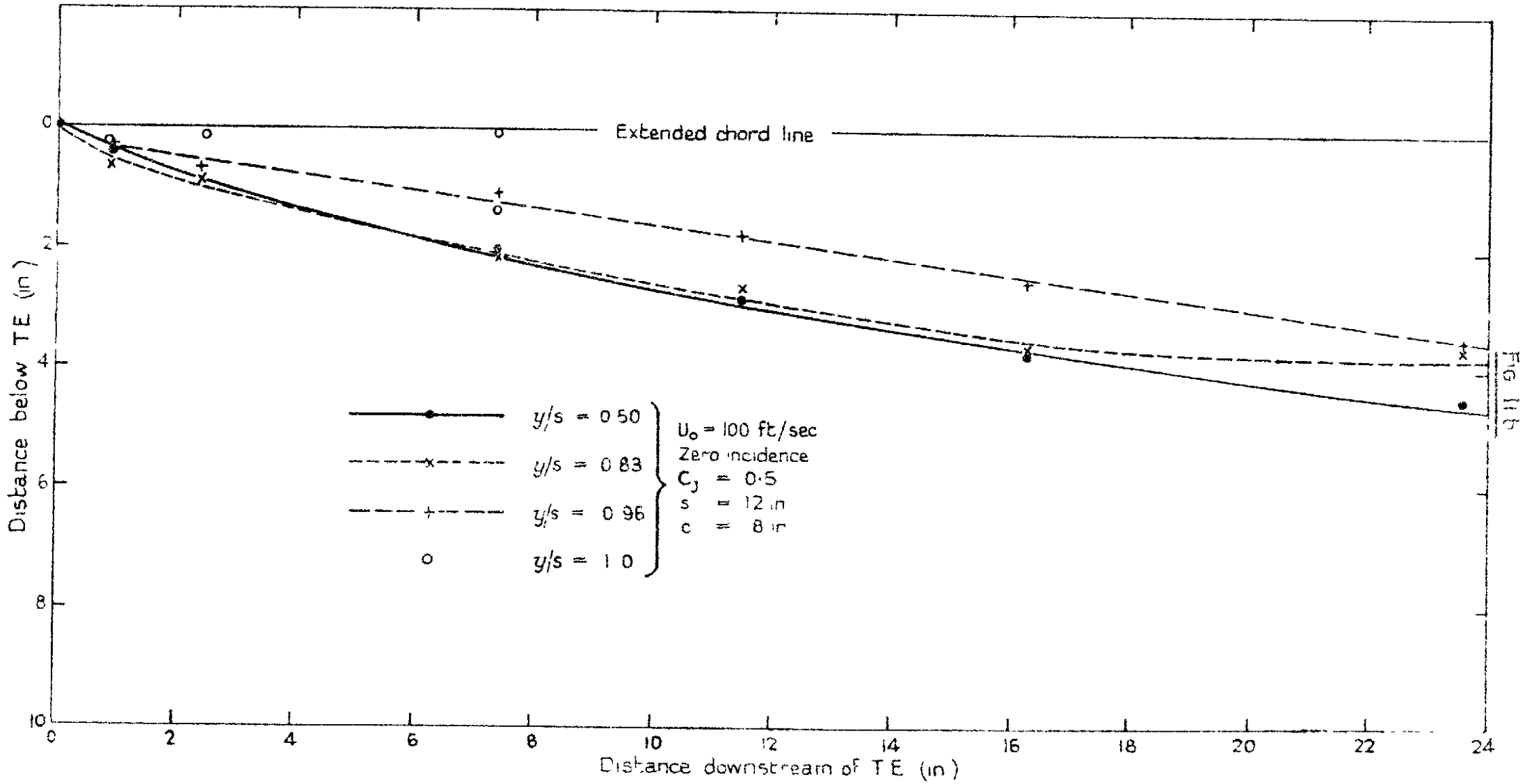

Fig 11b

Spanwise variation of mean line of jet

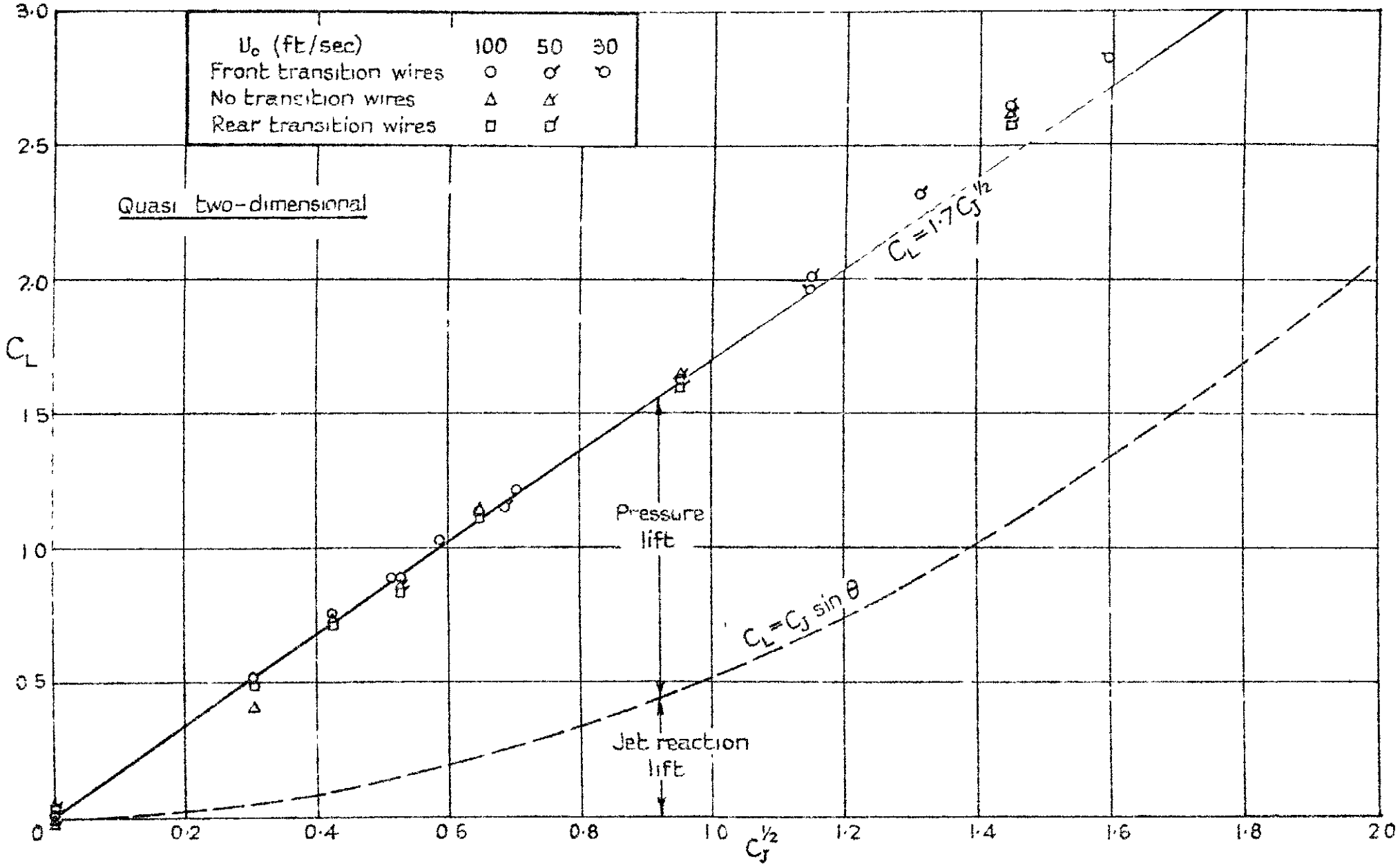

Variation of total lift C_L with $C_J^{1/2}$ at zero incidence

FIG. 12a

Quasi two-dimensional

$\alpha°$	U_0 ft/sec	
	100	50
11 5	▽	▽
6 5	△	△
0	○	○
−3 5	×	×

$\alpha = 11\,5°$

6 5°

0°

−3 5°

C_L

45 40 35 30 25 20 15 10 05 0 −0 5

0 0·2 0·4 0·6 0·8 1·0 1·2 1·4 1·6 1·8 2·0

$C_J^{1/2}$

Variation of total lift C_L with $C_J^{1/2}$ at constant incidence

Fig 13.

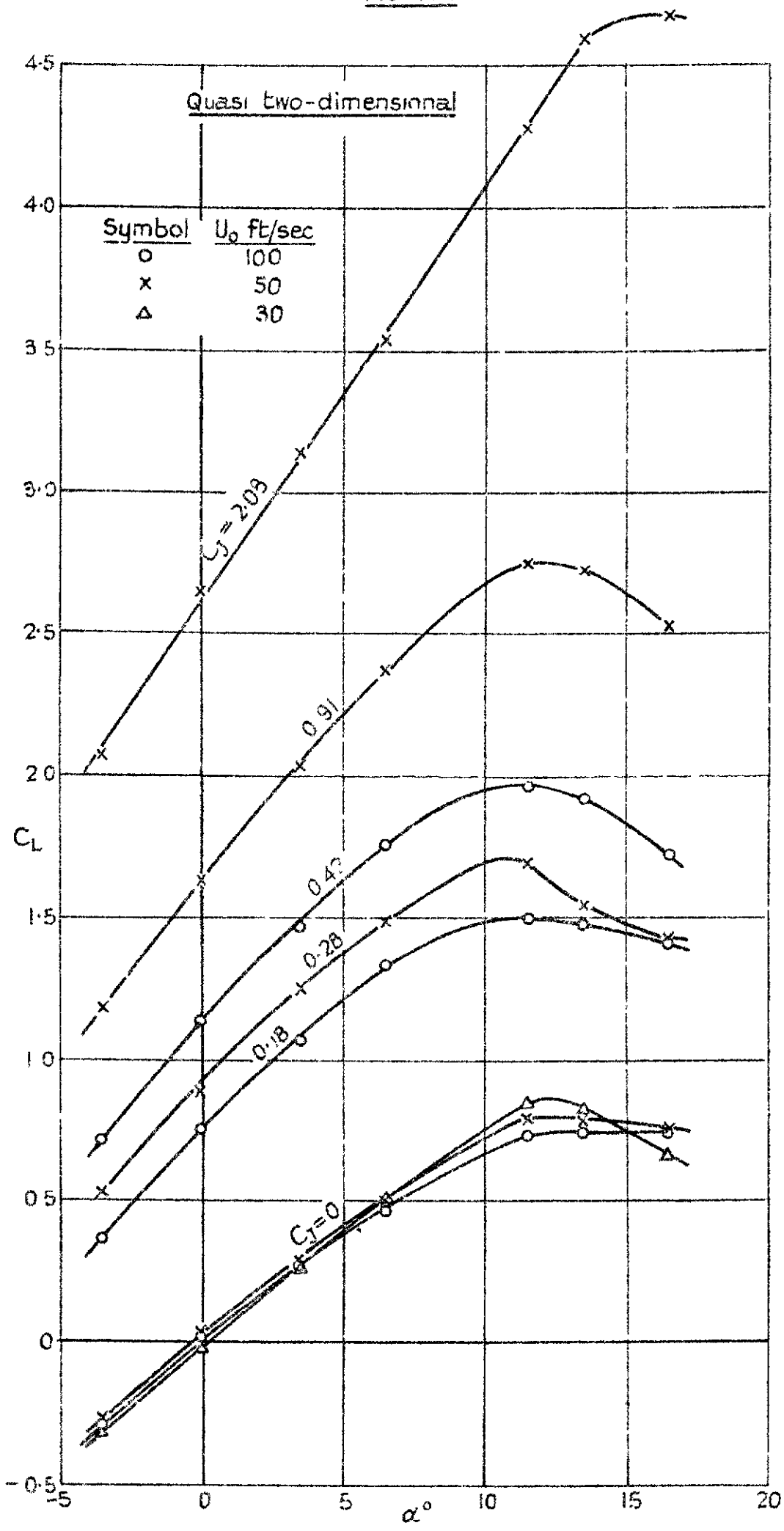

Variation of total lift with incidence at constant C_J

(Ref. 4A/6/18)

FIG. 14.

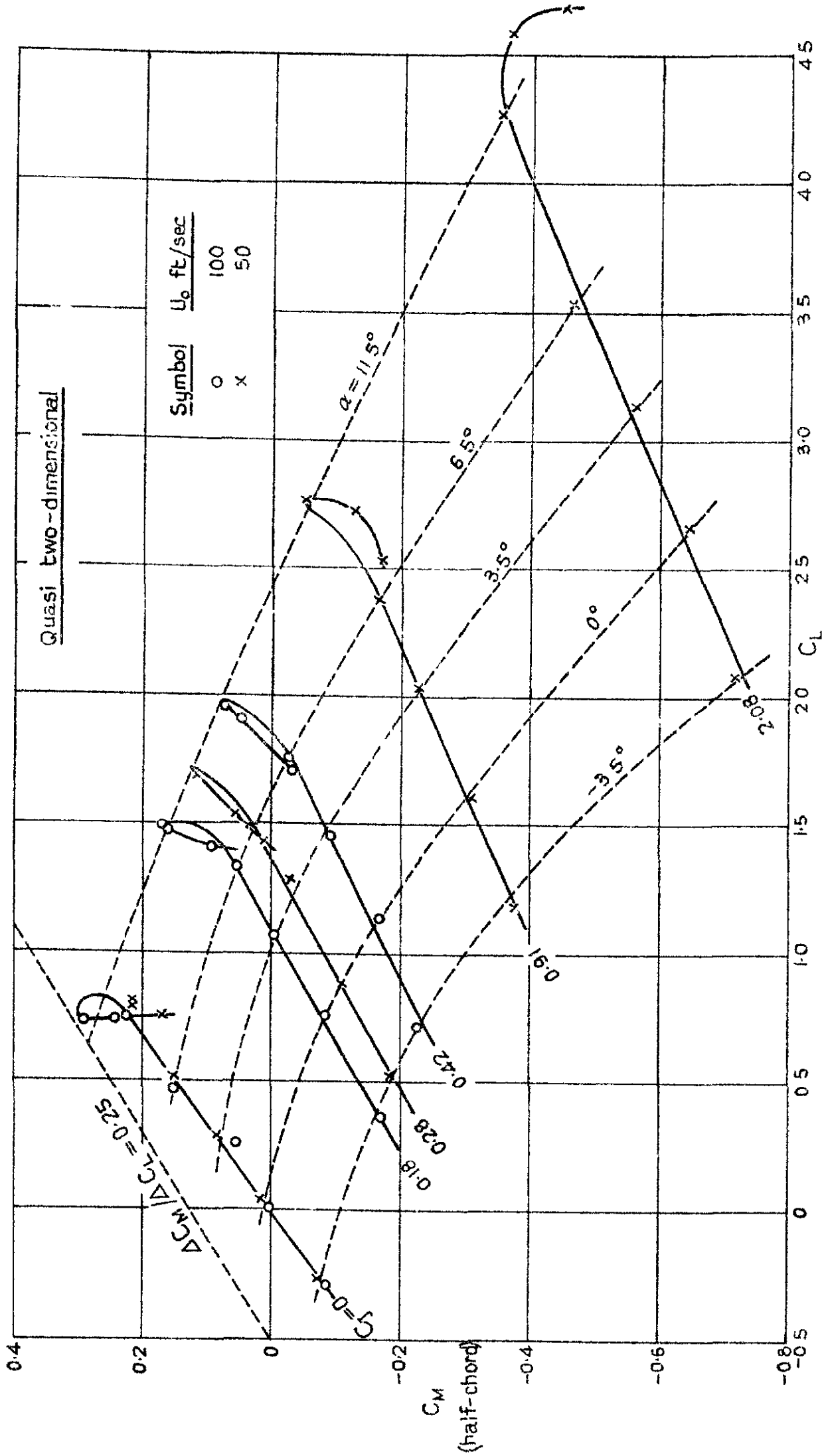

Variation of total pitching moment with total lift

FIG 15

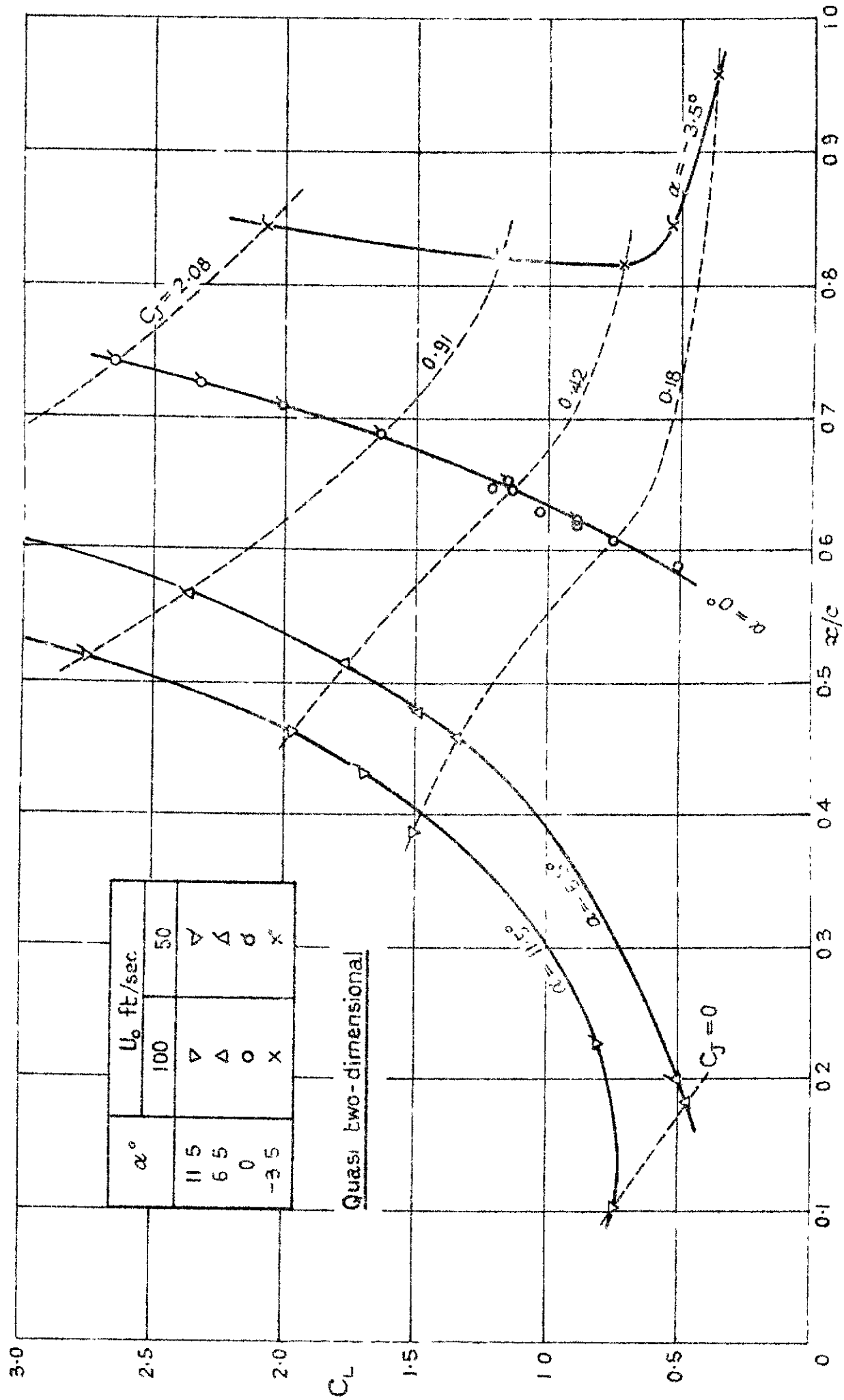

Variation in position of centre of total lift.

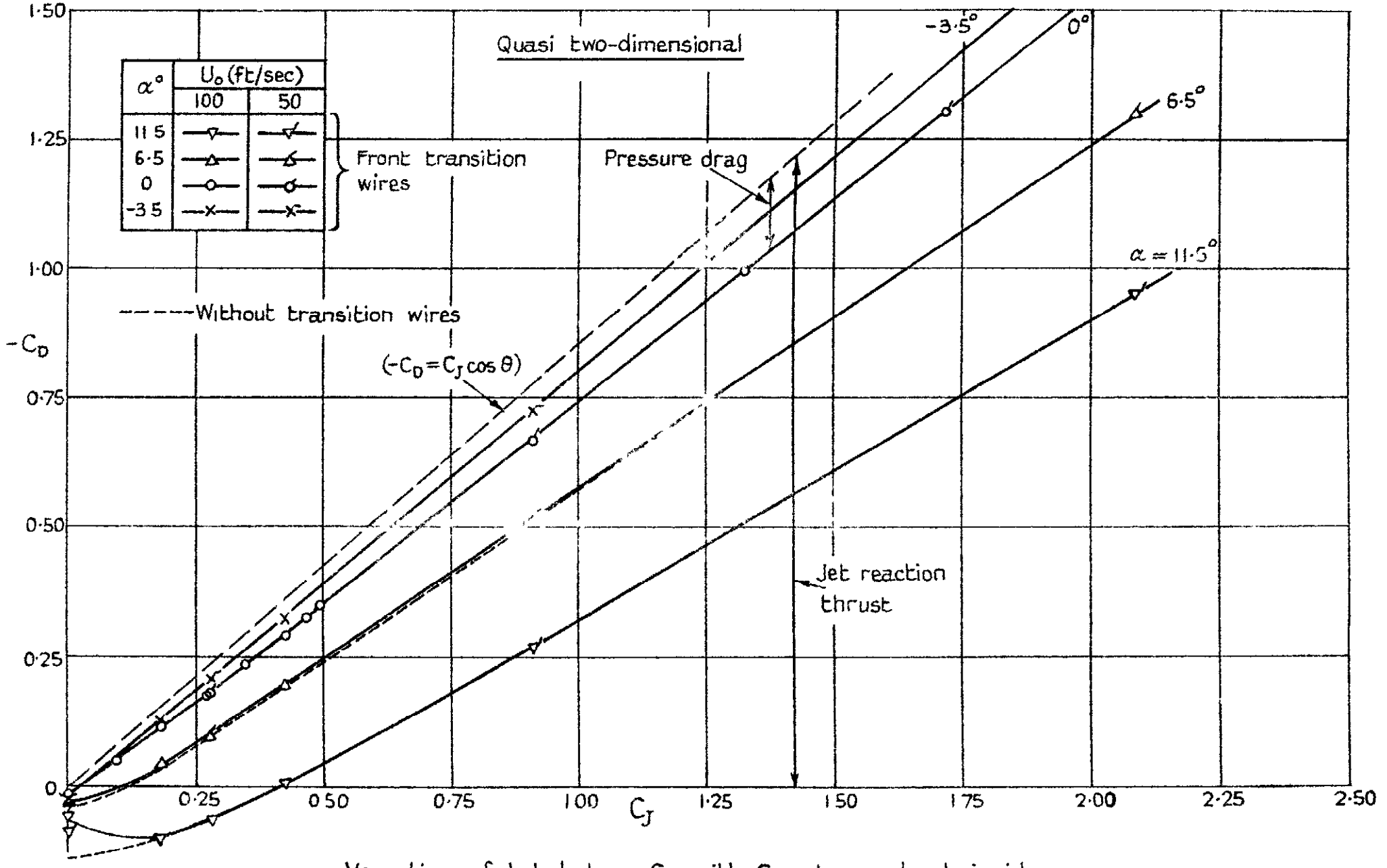

Variation of total drag C_D with C_J at constant incidence

Fig. 15 a.

Fig. 16 b

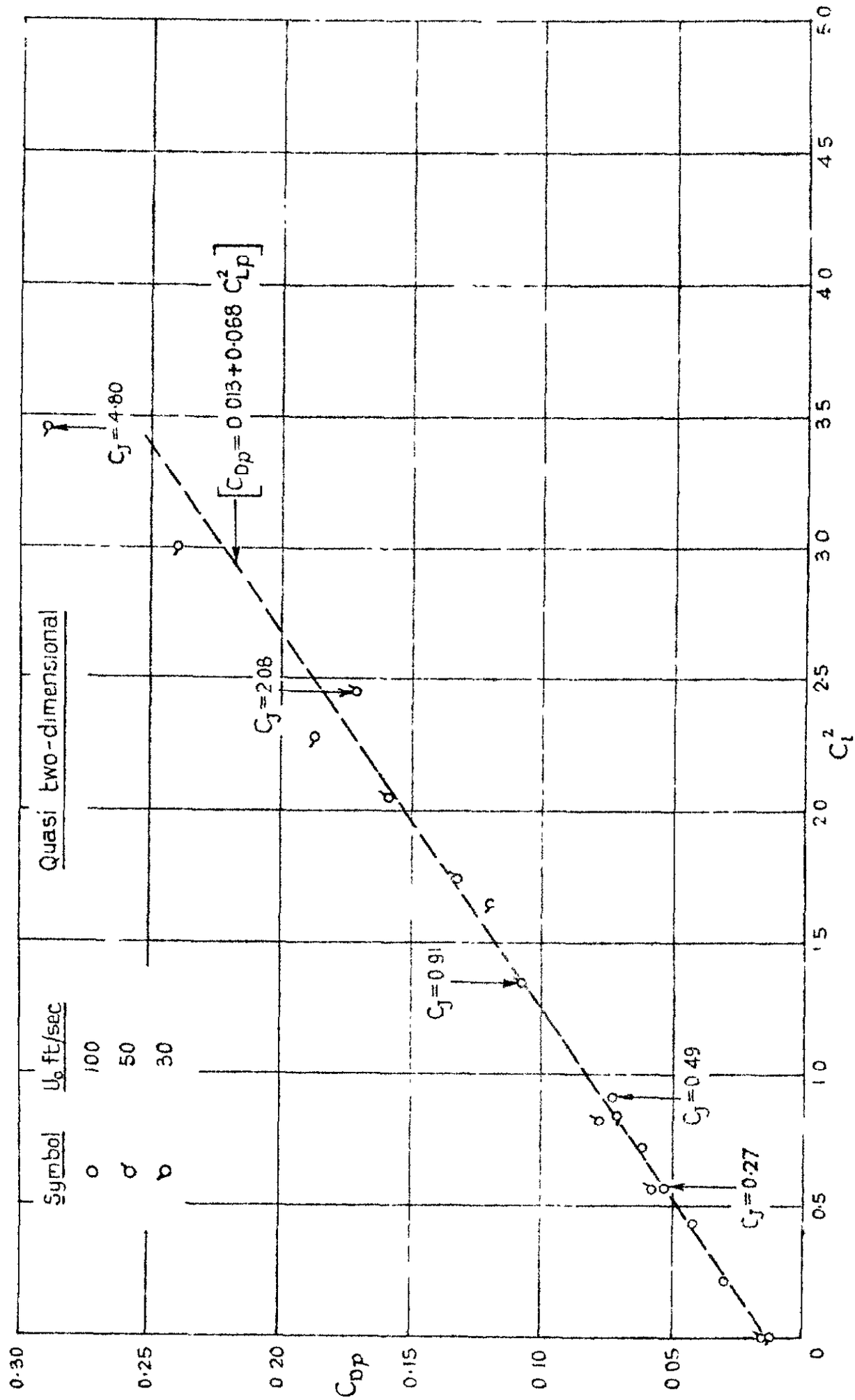

Variation of pressure drag C_D with C_l^2 at zero incidence.

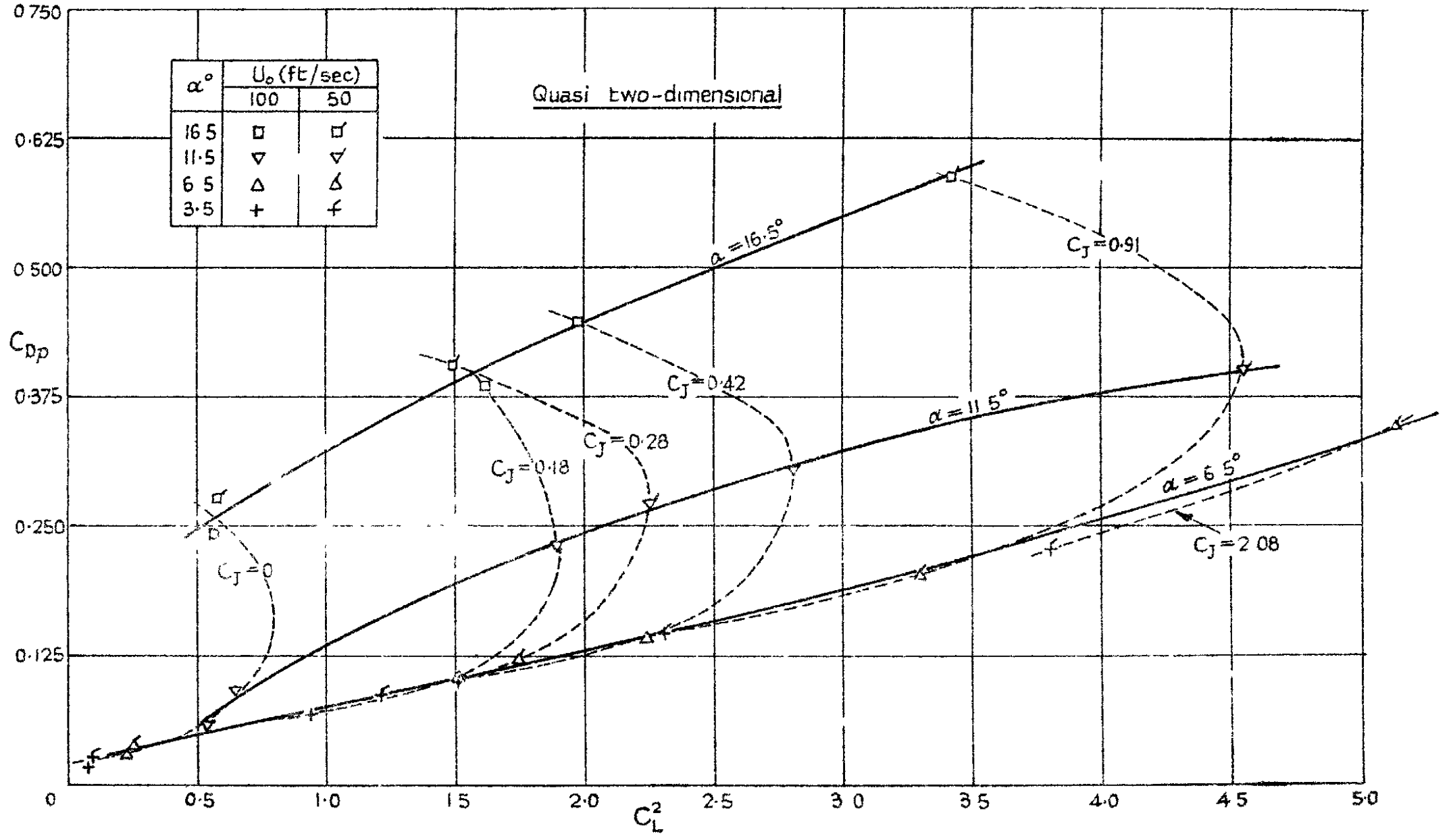

Fig. 16c

Variation of pressure drag C_{Dp} with C_{Lp}^2

FIG. 16 d

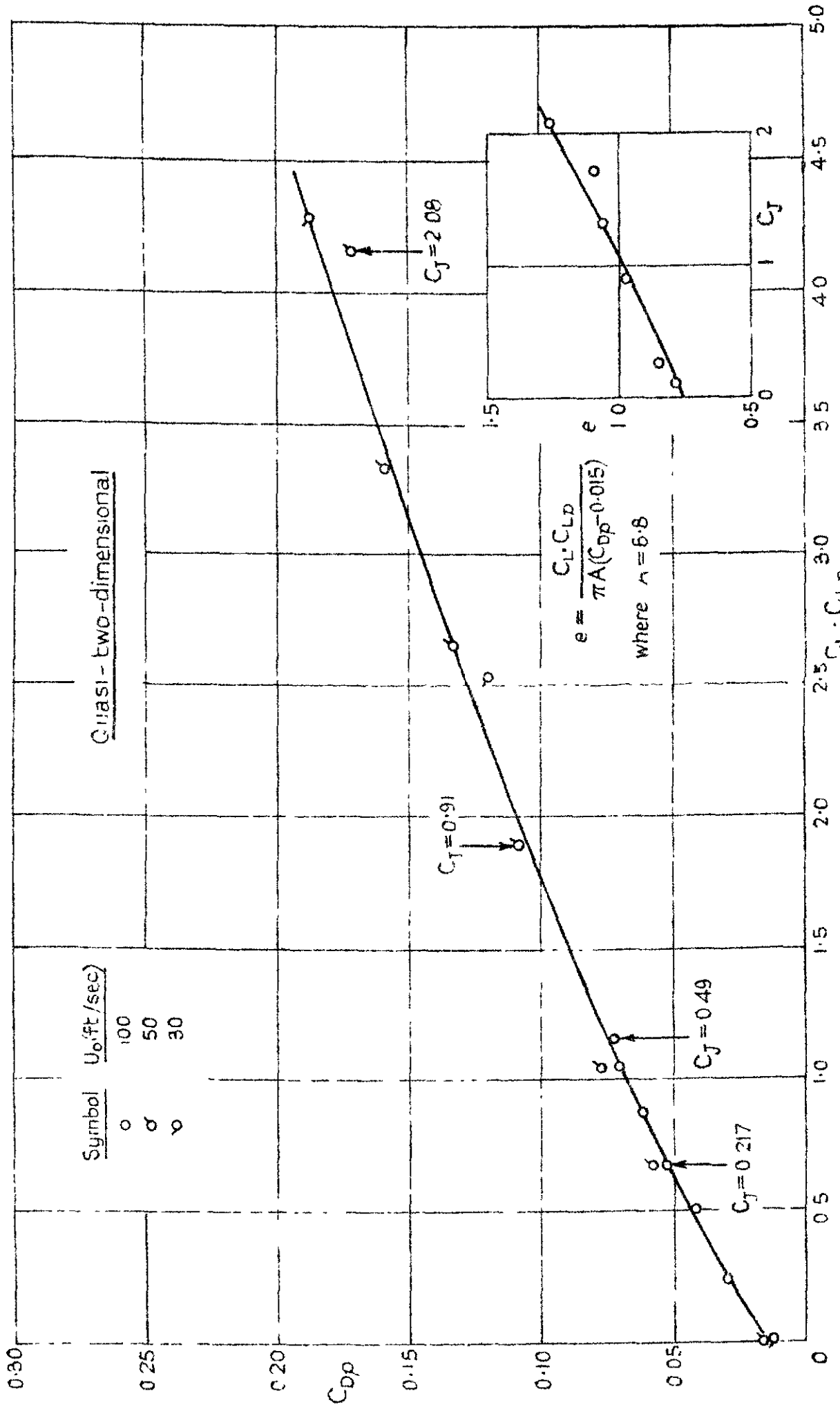

Variation of pressure drag C_{Dp} with $C_L \cdot C_{Lp}$ at zero incidence

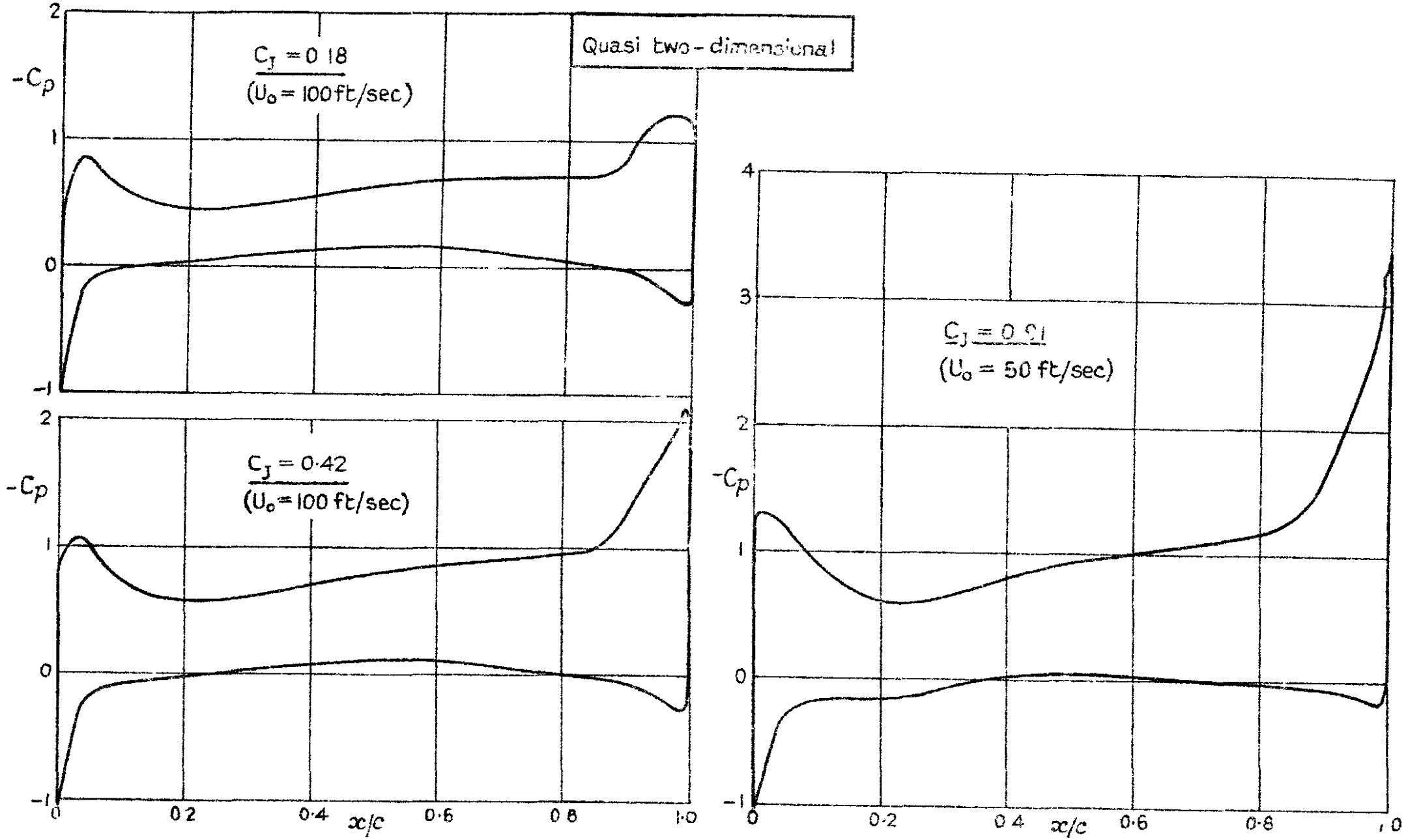

Fig. 17 a.

Chordwise pressure distributions at zero incidence – Variation with C_J.

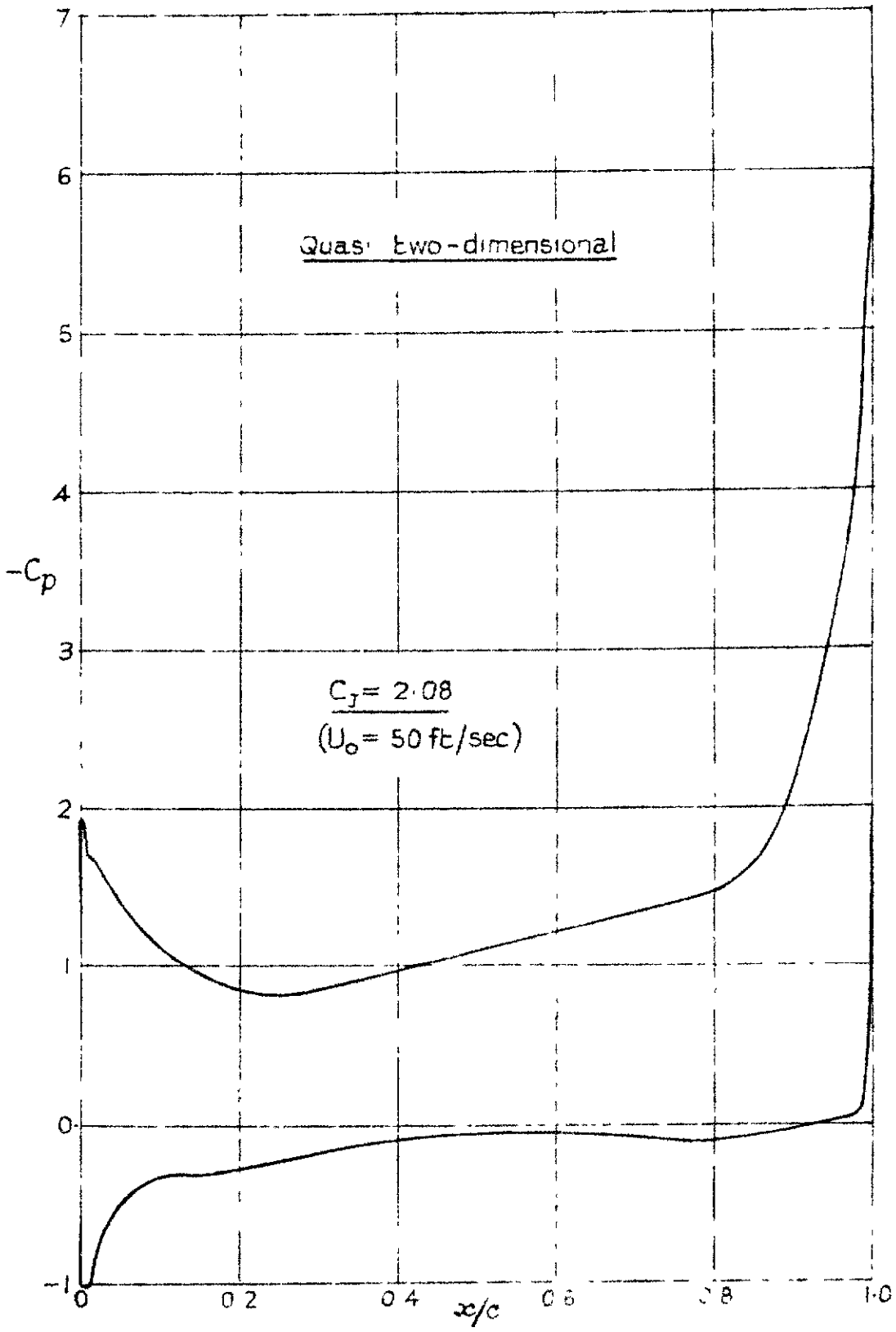

Chordwise pressure distribution at zero incidence – Variation with C_J

FIG. 18 a.

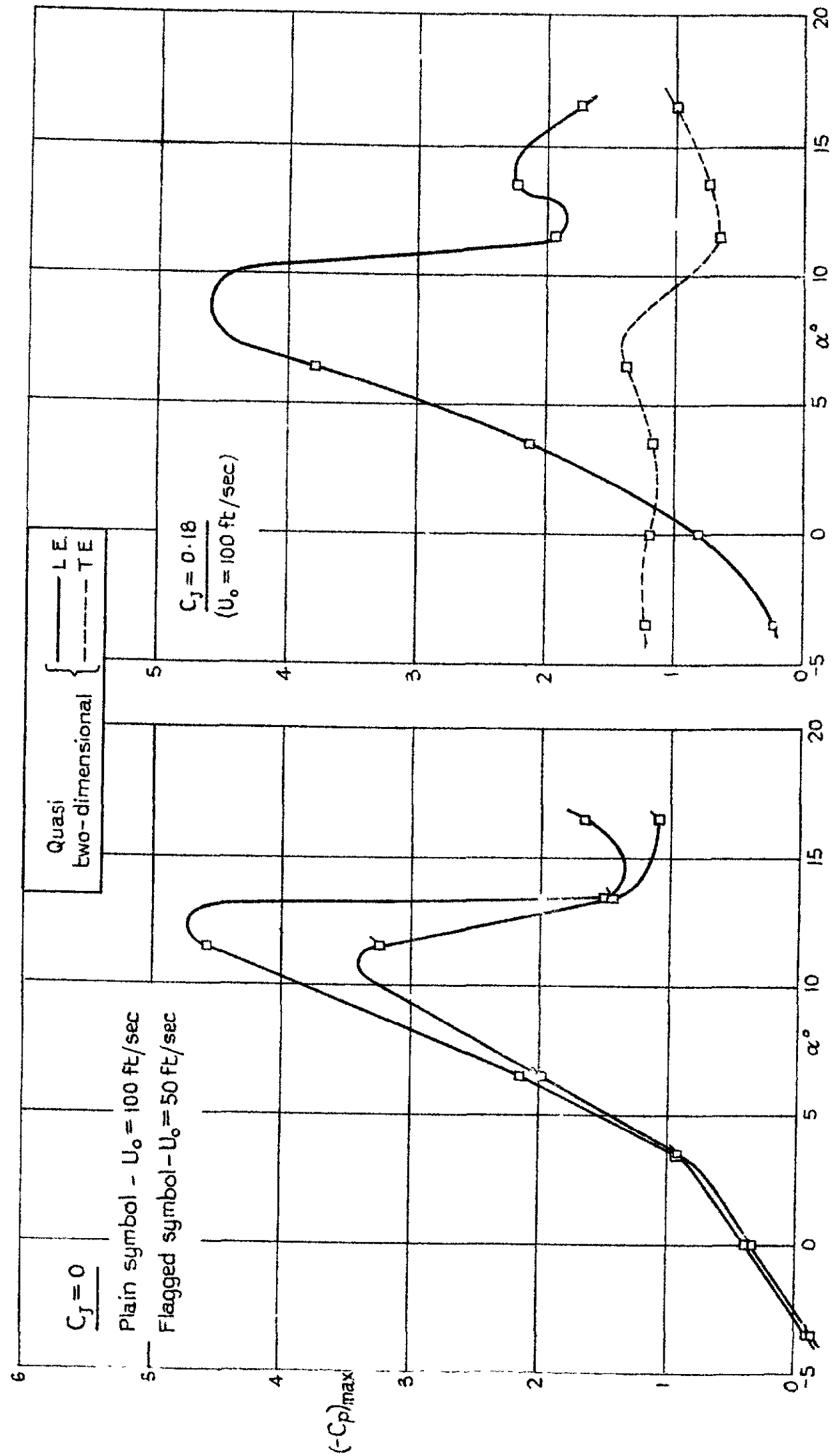

Variation of peak suctions near L.E and T.E.

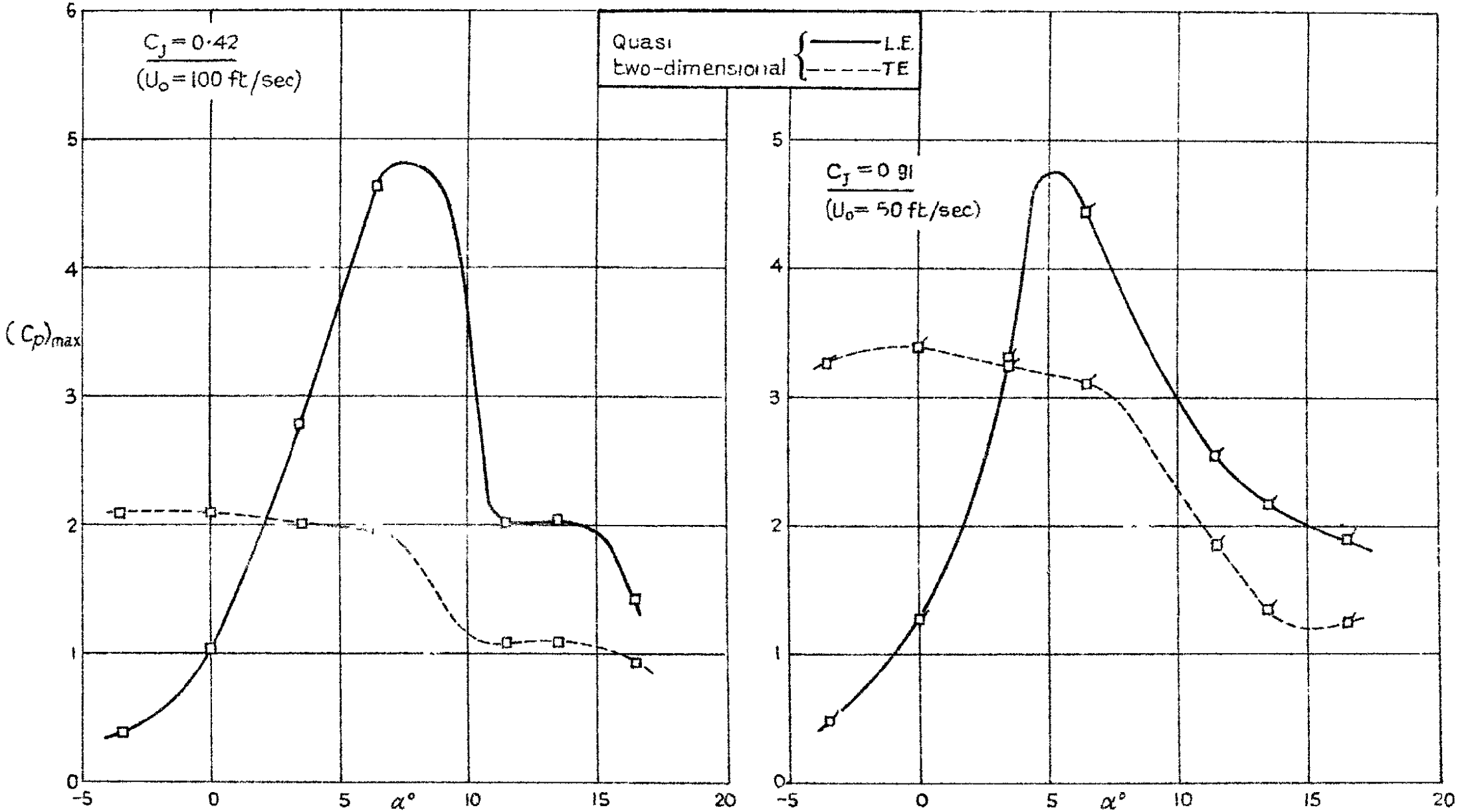

Fig. 18b

Variation of peak suction near L.E. and T.E.

FIG. 18c.

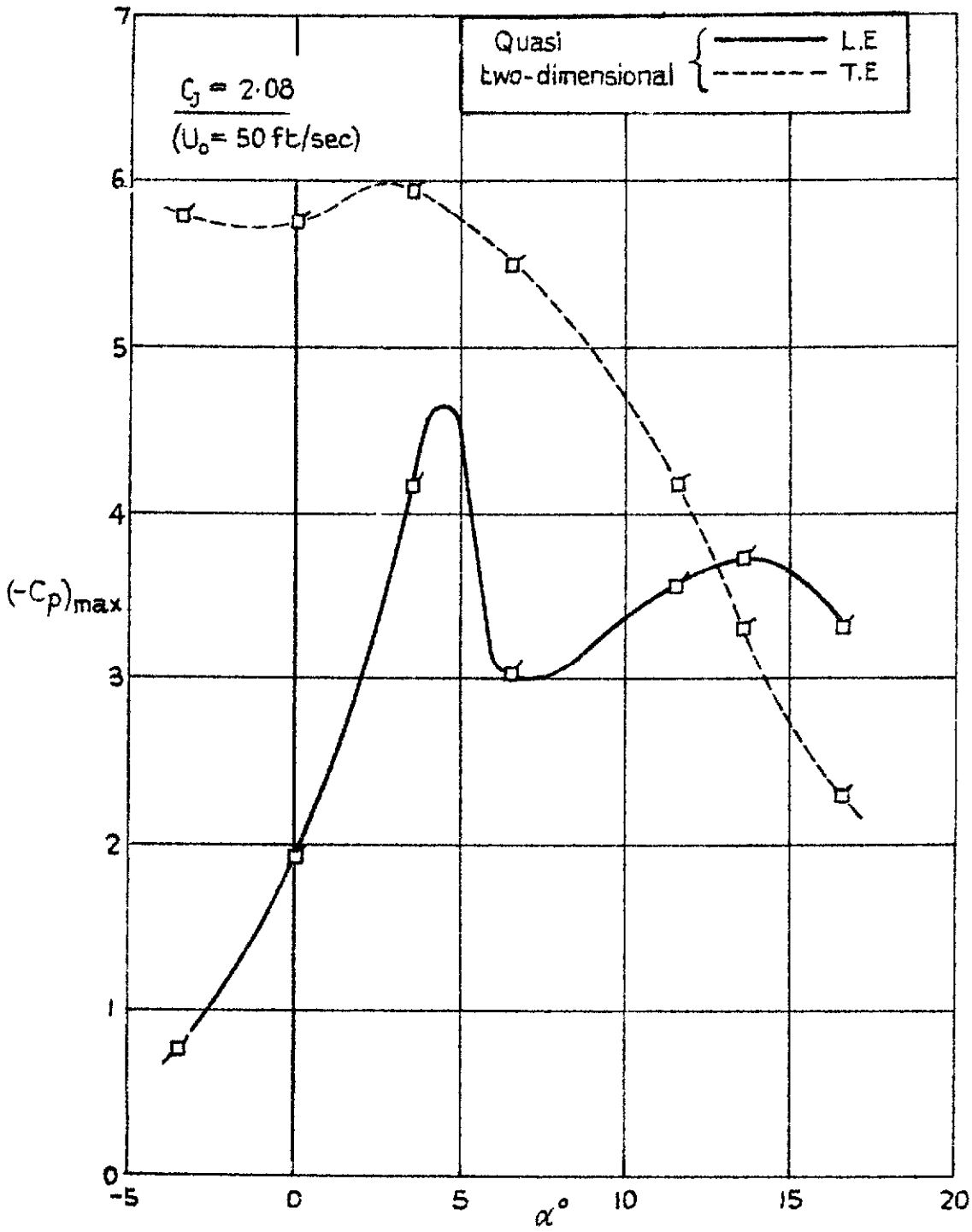

Variation of peak suction near L.E. and T.E.

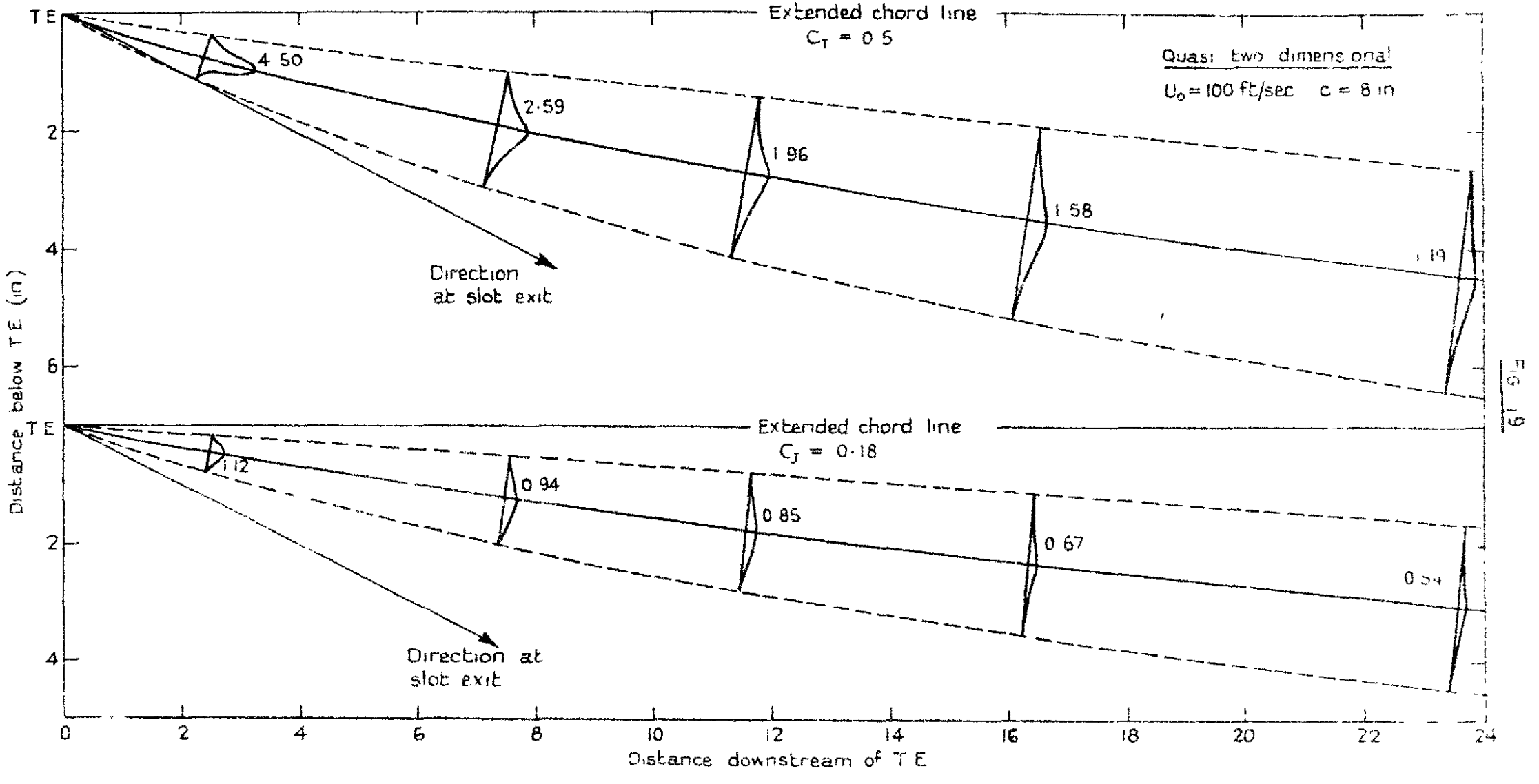

Fig 19

Mean line and total head profiles of jet

C.P. No. 304
(17,990)
A.R.C Technical Report

Printed and published by
HER MAJESTY'S STATIONERY OFFICE

To be purchased from
York House, Kingsway, London W C 2
423 Oxford Street, London W.1
P O Box 569, London S.E.1
13A Castle Street, Edinburgh 2
109 St. Mary Street, Cardiff
39 King Street, Manchester 2
Tower Lane, Bristol 1
2 Edmund Street, Birmingham 3
80 Chichester Street, Belfast
or through any bookseller

Printed in Great Britain

S.O Code No. 23-9010-4

C.P. No. 304